


Article (refereed) - postprint

Lian, Xu; Piao, Shilong; Chen, Anping; Huntingford, Chris ; Fu, Bojie; Li, Laurent Z.X.; Huang, Jianping; Sheffield, Justin; Berg, Alexis M.; Keenan, Trevor F.; McVicar, Tim R.; Wada, Yoshihide; Wang, Xuhui; Wang, Tao; Yang, Yuting; Roderick, Michael L.. 2021. **Multifaceted characteristics of dryland aridity changes in a warming world.** *Nature Reviews Earth & Environment*, 2. 232-250. <https://doi.org/10.1038/s43017-021-00144-0>

© The Author(s), under exclusive licence to Springer Nature Limited 2020

For use in accordance with Nature Research's Terms of Reuse of archived manuscripts

This version is available at <http://nora.nerc.ac.uk/id/eprint/529945>

Copyright and other rights for material on this site are retained by the rights owners. Users should read the terms and conditions of use of this material at <https://nora.nerc.ac.uk/policies.html#access>.

This document is the authors' final manuscript version of the journal article, incorporating any revisions agreed during the peer review process. There may be differences between this and the publisher's version. You are advised to consult the publisher's version if you wish to cite from this article.

The definitive version is available at <https://www.nature.com/>

Contact UKCEH NORA team at
noraceh@ceh.ac.uk

Multifaceted characteristics of dryland aridity changes in a warming world

Xu Lian¹, Shilong Piao^{1,2,3,†}, Anping Chen^{4,5,6}, Chris Huntingford⁷, Bojie Fu^{8,9}, Laurent Z. X. Li¹⁰, Jianping Huang¹¹, Justin Sheffield¹², Alexis M. Berg¹³, Trevor F. Keenan^{14,15}, Tim R. McVicar^{16,17}, Yoshihide Wada¹⁸, Xuhui Wang¹, Tao Wang², Yuting Yang¹⁹ and Michael L. Roderick^{17,20}

¹ Sino-French Institute for Earth System Science, College of Urban and Environmental Sciences, Peking University, Beijing, China.

² Key Laboratory of Alpine Ecology, Institute of Tibetan Plateau Research, Chinese Academy of Sciences, Beijing, China.

³ Center for Excellence in Tibetan Earth Science, Chinese Academy of Sciences, Beijing, China.

⁴ Department of Biology, Colorado State University, Fort Collins, CO, USA.

⁵ Graduate Degree Program in Ecology, Colorado State University, Fort Collins, CO, USA.

⁶ Woodwell Climate Research Center, Falmouth, MA, USA.

⁷ Centre for Ecology and Hydrology, Wallingford, UK.

⁸ State Key Laboratory of Urban and Regional Ecology, Research Center for Eco-Environmental Sciences, Chinese Academy of Sciences, Beijing, China.

⁹ State Key Laboratory of Earth Surface Processes and Resource Ecology, Faculty of Geographical Science, Beijing Normal University, Beijing, China.

¹⁰ Laboratoire de Météorologie Dynamique, CNRS, Sorbonne Université, Ecole Normale Supérieure, Ecole Polytechnique, Paris, France.

¹¹ Key Laboratory for Semi-Arid Climate Change of the Ministry of Education, College of Atmospheric Sciences, Lanzhou University, Lanzhou, China.

23 ¹² Department of Geography, University of Southampton, Southampton, UK.

24 ¹³ Department of Earth and Planetary Sciences, Harvard University, Cambridge, MA, USA.

25 ¹⁴ Earth and Environmental Sciences Area, Lawrence Berkeley National Laboratory, Berkeley,
26 CA, USA.

27 ¹⁵ Department of Environmental Science Policy and Management, University of California
28 Berkeley, Berkeley, CA, USA.

29 ¹⁶ CSIRO Land and Water, Canberra, ACT, Australia.

30 ¹⁷ Australian Research Council Centre of Excellence for Climate Extremes, Canberra, ACT,
31 Australia.

32 ¹⁸ International Institute for Applied Systems Analysis, Laxenburg, Austria.

33 ¹⁹ State Key Laboratory of Hydrosience and Engineering, Department of Hydraulic
34 Engineering, Tsinghua University, Beijing, China.

35 ²⁰ Research School of Earth Sciences, Australian National University, Canberra, ACT, Australia.

36 † email: slpiao@pku.edu.cn

37

38 **Abstract**

39 **Drylands are an essential component of the Earth system and are among the most**
40 **vulnerable to climate change. In this Review, we synthesize observational and modelling**
41 **evidence to demonstrate emerging differences in dryland aridity dependent on the specific**
42 **metric considered. Although warming heightens vapour-pressure deficit and, thus,**
43 **atmospheric demand for water in both the observations and projections, these changes do**
44 **not wholly propagate to exacerbate soil moisture and runoff deficits. Moreover, counter-**
45 **intuitively, many arid ecosystems have exhibited significant greening and enhanced**
46 **vegetation productivity since the 1980s. Such divergence between atmospheric and**
47 **ecohydrological aridity changes can primarily be related to moisture limitations by dry**
48 **soils and plant physiological regulations of evapotranspiration under elevated CO₂. The**
49 **latter process ameliorates water stress on plant growth and decelerates warming-**
50 **enhanced water losses from soils, while simultaneously warming and drying the near-**
51 **surface air. We place these climate-induced aridity changes in the context of exacerbated**
52 **water scarcity driven by rapidly increasing anthropogenic needs for freshwater to support**
53 **population growth and economic development. Under future warming, dryland**
54 **ecosystems might respond nonlinearly, caused by, for example, complex ecosystem-**
55 **hydrology-human interactions and increased mortality risks from drought and heat stress,**
56 **which is a foremost priority for future research.**

57

58 [H1] Introduction

59 Drylands describe regions subject to permanent or seasonal water deficiency, which currently
60 occupy ~42% of global land surface¹⁻⁴. They are typically located in subtropical regions
61 characterised by air mass divergence, in the rain shadow of mountain chains or in the middle
62 of continental landmasses⁵ (**Fig. 1**). Dryland ecosystems have a critical role in the global carbon
63 cycle, dominating the trend and variability of global terrestrial carbon sink owing to their high
64 sensitivity to inter-annual climate variability⁶. Moreover, they are home to ~30% of the world's
65 endangered and endemic species^{7,8}, and are thus critical to global biodiversity conservation
66 efforts. Drylands also provide staple food, cotton, timbers and livestock to support nearly 2.5
67 billion people^{1,3,8}, among whom about half live below the United Nations poverty line.

68 The sustainability of ecosystem services and societal goods provided by global drylands,
69 however, is threatened by ongoing anthropogenic warming^{1,2,9}. Indeed, the limited socio-
70 economic capacity for adaptation and mitigation^{9,10}, together with the faster-than-average
71 warming rate^{2,11,12}, makes drylands among the most vulnerable regions to climate change. As
72 such, concerns about the fate of dryland socio-ecological systems have been a priority for
73 important global initiatives, including: The Global Dryland Ecosystem Programme¹³; the
74 Intergovernmental Science-Policy Platform on Biodiversity and Ecosystem Services¹⁴; the
75 United Nations Convention on Biological Diversity¹⁵; the United Nations Sustainability
76 Development Goals¹⁶; and the Intergovernmental Panel on Climate Change³.

77 A surge of research has therefore emerged to assess dryland changes in the past and predict
78 their future trajectories, the findings of which are highly contradictory. For example, numerous
79 studies suggest that global drylands have become more arid^{10,17-26}, yet others show the same

80 regions experiencing greening and enhanced vegetation activity^{6,27-33}. This apparent
81 inconsistency stems from different interpretations of aridity – the state of insufficient water
82 supply to meet demand^{34,35} – dependent on whether it is used in an atmospheric, agricultural,
83 hydrologic or ecological context (**Box 1**). The associated demand and supply sides of aridity,
84 as well as the physical and/or biological processes driving changes of both sides, vary
85 considerably among these different interpretations.

86 In this Review, we reconcile disagreements between aridity metrics by acknowledging the
87 multifaceted nature of water supply and demand for the atmosphere, hydrological systems,
88 ecosystems and human society over global drylands, as well as their interconnections³⁵⁻³⁷,
89 knowledge of which will allow for more effective adaptation policies. We first provide an
90 overview of how aridity and the extent of global drylands have changed since the 1950s and
91 are projected to change in the future, presenting contrasting findings according to atmospheric,
92 agricultural, hydrological or ecological dryland definitions. We next discuss the attribution of
93 aridity changes to physical and physiological processes within the dryland system, arguing that
94 strong soil moisture limitations, together with ecosystem physiological regulations of
95 hydrological cycles under rising atmospheric CO₂, can explain the apparent conflicting
96 viewpoints. We then outline the central role of humans in water resource utilisation and evaluate
97 dryland management policy decisions under the intensification of ecosystem-hydrology-human
98 interactions. We end with a forward-looking perspective on future dryland research.

99

100 **[H1] Historical aridity changes in drylands**

101 The growth of global data from remote sensing and in-situ networks, along with sophisticated
102 climate-carbon cycle modelling, provides valuable new datasets and tools for assessing long-
103 term surface aridity changes^{38,39} (**Supplementary Table 1**). A large body of research uses the
104 aridity index, $AI^{10,17,21,22,24,40-43}$, which represents the balance between water received by the
105 land surface (precipitation) and that demanded by the atmosphere (potential evapotranspiration,
106 PET) (**Box 1**). However, it has been suggested that AI could be problematic in depicting surface
107 aridity changes, being too simplistic to capture the full complexity of aridity^{40,44,45}.

108 Hence, there is an increasing recognition that aridity should be evaluated using a more diverse
109 representation of water demand and supply for different land surface processes^{36,40,46}. Four
110 alternative aridity metrics have thus been increasingly employed, including: vapour pressure
111 deficit (VPD), which measures the atmospheric water demand; soil moisture, which describes
112 the soil water supply to support ecosystem function and agricultural production; runoff, which
113 signifies the volume of freshwater available for drinking, irrigation, industry and other societal
114 needs; and vegetation productivity and/or greenness, a robust indicator of ecological aridity
115 given the primary role of water in determining dryland vegetation productivity²⁸.

116 With these five aridity metrics, as quantified by observations and state-of-the-art model
117 simulations (12 offline dynamic global vegetation models, DGVMs, and 23 Earth system
118 models, ESMs, from the Coupled Model Intercomparison Project Phase 5, CMIP5;
119 **Supplementary Tables 2 & 3**), two approaches are used to assess dryland aridity changes since
120 the 1950s and projections into the future (**Fig. 2**). The first takes zonal-average values of
121 different aridity metrics over global drylands, while assuming a fixed global dryland extent (as
122 in **Fig. 1**). The second calculates the evolving fraction of global water-stressed area, applying a

123 fixed threshold to each aridity metric to derive a temporally-variable dryland extent
124 (**Supplementary Methods; Supplementary Figs. 1-3**). In the second approach, the fraction of
125 global water-stressed area is denoted as $f_{\text{atm}}, f_{\text{AI}}, f_{\text{soil}}, f_{\text{hyd}}, f_{\text{veg}}$, for aridity metrics defined by VPD,
126 AI, soil moisture, runoff and vegetation productivity, respectively. Aridity changes of global
127 drylands using these different metrics are now quantified and compared.

128

129 **[H2] Ubiquitous atmospheric drying**

130 VPD is defined as the difference between saturated water vapour pressure (which increases
131 exponentially with air temperature) and actual water vapour pressure (which is a function of air
132 humidity). Hence, VPD measures how far the air is from thermodynamic equilibrium, with high
133 values related to strong atmospheric demand for water from land and/or water surfaces.
134 Research into VPD changes consistently indicates an increasing trend of global dryland
135 atmospheric aridity⁴⁷⁻⁴⁹, as confirmed by various observational datasets (**Supplementary**
136 **Figure 4**). On average, global dryland VPD shows a statistically significant increase of 0.012
137 ± 0.001 kPa decade⁻¹ ($p < 0.05$) over 1948-2016 (**Fig. 2a; Table 1**), as also reproduced by
138 ESMs (0.015 ± 0.002 kPa decade⁻¹, $p < 0.05$). Consistent with the overall VPD increase, the
139 global dryland area exposed to atmospheric water stress, as defined by VPD-based f_{atm} ,
140 similarly exhibits an increasing trend of $0.55 \pm 0.11\%$ decade⁻¹ ($p < 0.01$) over the same time
141 period (**Fig. 2f, Table 1**). As dryland surfaces warm 20-40% faster than humid regions⁴¹, the
142 increase in VPD is amongst the highest values on the global land surface, ~25% higher than
143 humid regions^{48,49}.

144

145 **[H2] Land surface drying characterised by the standard Aridity Index**

146 Traditionally, the most widely used metric to examine surface aridity was the AI^{10,21,24,42},
147 whereby a lower value corresponds to higher aridity, and is often interpreted as a higher risk of
148 desertification and land degradation^{3,10,50-52}. Observational and modeling-based AI studies
149 generally point to an enhanced drying trend since the pre-industrial era, signifying an expansion
150 of dryland area (as defined by a standard threshold of $AI \leq 0.65$)^{10,22,24} (**Supplementary Table**
151 **1**). For example, gauge-based precipitation and reanalysis-based PET data suggest a 2.4×10^6
152 km² expansion of global drylands when comparing 1991–2005 to the 1950s (ref. ²⁴), the
153 strongest regional increases of which occurred in southern Africa, the Sahel and North
154 China^{10,24}. This surface drying trend is confirmed through analyses using multiple combinations
155 of precipitation and PET datasets (**Fig. 2b**), translating into an ensemble mean global expansion
156 of dryland area (f_{AI}) by $0.13 \pm 0.06\%$ decade⁻¹ ($p < 0.05$) over 1948-2016 (**Fig. 2g, Table 1**).
157 However, the reported dryland aridity increase and dryland expansion are highly sensitive to
158 selected inputs of observational data products^{38,53}. For instance, the magnitude of the estimated
159 expansion rate has a large spread across different data streams, ranging from near zero to 0.60%
160 decade⁻¹ (**Table 1**). The previously reported rate of 0.57% decade⁻¹ (refs. ^{10,24}) falls into this
161 range but is close to the upper boundary.

162 While multi-data combinations provide a complete assessment of possible AI changes, they
163 cannot ensure the physical consistency between precipitation and other meteorological
164 variables involved in PET calculation⁵³. Assessments with climatic diagnostics from ESMs
165 generally do not have this physical inconsistency. Indeed, the observed AI decrease and

167 $\pm 0.03\% \text{ decade}^{-1}$ ($p < 0.05$) during 1948-2005
168 (**Fig. 2g, Table 1**), consistent with the ensemble mean of multiple empirical data combinations
169 ($0.13 \pm 0.06\% \text{ decade}^{-1}$). For both observations and models, the expanding rate of global
170 dryland extent based on AI is much slower than that based on VPD for the same period (**Figs.**
171 **2f, g**).

172 In addition, the AI is commonly calculated using the Penman-Monteith (PM) equation (**Box 1**),
173 now thought to overestimate PET changes under elevated CO₂ because it incorrectly assumes a
174 fixed resistance for vegetated surfaces^{40,45,54,55}. The introduction of a CO₂-responsive surface
175 resistance to the PM-based PET parameterization lowers PET increases (though it is still larger
176 than concurrent precipitation increases⁴⁰), and the resultant AI shows higher consistency with
177 modelled hydrological changes⁴⁵. Accounting for the CO₂ effect in the PET formulization thus
178 leads to a ~40% reduction in the estimated increase in AI-based dryland extent during 1948-
179 2016. As such, the resulting long-term trend becomes statistically insignificant at $0.08 \pm 0.06\%$
180 decade^{-1} (**Fig. 2g, Table 1**). However, caution is needed when utilizing the modified PET model
181 in dryland assessments as the model-based estimate of CO₂ effect on surface resistance has not
182 been experimentally validated⁴⁵. With this limitation in mind, it is anticipated that the CO₂-
183 modified PET model underestimates dryland PET increase and, thus, the rate of dryland
184 expansion. Therefore, the rate of AI-based dryland expansion should fall between the estimates
185 with and without accounting for the CO₂ impacts on PET, that is, between 0.08 and 0.13%
186 decade^{-1} .

187

188 **[H2] Relatively weak total-column soil moisture drying**

189 Soil moisture levels determine water stress for natural and agricultural ecosystems. Remote
190 sensing by microwave and gravimetric sensors, and its application in numerical land data
191 assimilation schemes, now offers a useful way to monitor soil moisture dynamics at large spatial
192 scales. However, there remain limitations with current technology including, limited vertical
193 sampling depth and low accuracy over densely vegetated surfaces for microwave-based
194 retrievals^{56,57}. Hence, compared to the more robust finding of aridification and dryland
195 expansion based on VPD or AI, aridity changes based on soil moisture often show divergent
196 signs, depending on the data used, the period investigated, and the soil depth involved.

197 Using microwave satellite observations of near-surface soil moisture, it is estimated that 38.4%
198 of global drylands have experienced a significant drying trend since 1979, while only 2.9%
199 showed a wetting trend⁵⁸. However, other observation-driven datasets of total-column (or root-
200 zone) soil moisture (such as GLEAM, TerraClimate and GLDAS, see **Supplementary**
201 **Methods**) consistently reveal an increasing trend for the same period (**Fig. 2c, Table 1**). The
202 divergence of soil moisture trends is likely because surface and deep-layer soil moistures are
203 controlled by different processes—warming-induced rise in evaporative demand drives the
204 reduction of surface soil moisture, whereas soil moisture in deep layers is more controlled by
205 antecedent moisture status and vegetation activities⁵⁹⁻⁶¹. Weaker drying in the root-zone
206 compared to the surface soil suggests that deep-rooted plants in drylands are less likely to suffer
207 severe soil moisture stress than shallow-rooted plants and crops.

208

209 Over 2002-2016, gravimetric sensors onboard NASA's Gravity Recovery and Climate
210 Experiment satellites, however, detect a robust decline of endorheic water storage²⁰ by about
211 106.3 Gt yr⁻¹, most of which is in drylands. Central Eurasia contributes most (69%) to this
212 decline, followed by the Sahara Desert, the dry Andes, Australia and western U.S., while water
213 gains were found in the Great Rift Valley and southern Africa²⁰. This signal of endorheic water
214 loss reflects an overall reduction of soil moisture, surface water and groundwater levels, likely
215 attributable to decadal or longer climate variability and human influence^{20,62}.

216 Despite strong model dependencies, soil moisture estimated by climate models also generally
217 show a decreasing trend over drylands^{59,63,64}. The model-derived trend is qualitatively similar
218 in pattern to the AI⁶³, and extends for both surface soils and the total soil column, although
219 being more significant for the former^{59,60}. As such, the global land area under (total-column)
220 soil moisture stress predicted by both DGVMs and CMIP5 ESMs is increasing at $0.09 \pm 0.05\%$
221 decade^{-1} ($p = 0.05$) and $0.05 \pm 0.02\% \text{decade}^{-1}$ ($p < 0.05$), respectively over 1948-2016 (**Fig. 2h,**
222 **Table 1**). The rate of dryland expansion inferred from modeled total soil moisture is
223 substantially smaller than that from VPD or AI. Hence, the increased atmospheric evaporative
224 demand has not fully translated to increased soil moisture deficits across all soil layers, despite
225 its dominance on the enhanced soil moisture deficits at the near-surface layer^{59,60}.

226

227 **[H2] Regionally divergent runoff changes**

228 Along with deep groundwater resources, surface runoff is an important source of freshwater for
229 societal demands of agricultural and industrial production in drylands. Unlike the ubiquitous

230 increase in surface aridity inferred from the VPD and AI metrics, runoff generally reveals
231 divergent regional changes^{44,65,66}, suggesting spatially heterogeneous hydro-climatic drivers
232 and runoff responses.

233 Surface runoff of most dryland rivers is decreasing^{19,65,67-69}. Indeed, through aggregating
234 streamflow records of the world's largest rivers flowing through drylands (**Supplementary**
235 **Table 4**), an overall declining trend in streamflow of $-0.19 \pm 0.12 \text{ mm yr}^{-1}$ ($p = 0.11$; or -11.9%)
236 is apparent during 1948-2016 (**Fig. 2d, Table 1**). In general, regions experiencing rapid runoff
237 decreases often overlap with those under intense human influences, such as the Yellow River
238 in North China⁶⁷, the Guadalquivir River in Spain, the Murray River in southeastern Australia
239 and the Indus River in Pakistan⁷⁰ (**Supplementary Table 4**). Simulations by both DGVMs and
240 CMIP5 ESMs agree with the observed overall decline (**Fig. 2d, Table 1**). Consequently, there
241 is an increase of modeled land area subject to hydrological aridity evaluated by runoff deficits
242 (f_{hyd}), reaching $0.06 \pm 0.07\% \text{ decade}^{-1}$ ($p > 0.10$) for DVGMs and $0.03 \pm 0.02\% \text{ decade}^{-1}$ ($p <$
243 0.10) for ESMs (**Fig. 2i, Table 1**). Achieving a high statistical significance is, however,
244 precluded by the strong decadal climate variability and spatial heterogeneity.

245 Nevertheless, increases in runoff have also been observed for about 20% of large rivers in arid
246 regions⁶⁵, such as the Daly River in north Australia and the Tana River in Kenya⁷⁰. This runoff
247 increase has been even more widespread since 1980s, driven by concurrent precipitation
248 increases, as supported by both observational streamflow records⁷⁰ and a gridded synthesis
249 runoff product⁷¹ (**Fig. 2i, Table 1**).

250

251 **[H2] Reduced water stress for dryland vegetation**

252 Increased VPD indicates a higher vapour-pressure gradient between leaves and the atmosphere,
253 enhancing water loss by plant transpiration^{49,72}. However, plants can also modify their water
254 need through physiological adjustments over both shorter and longer time scales, for example
255 through regulating stomatal conductance and changing leaf area, respectively^{19,32,37}. In drylands,
256 how well plants adapt to changing hydrological regimes, and consequently how well they grow,
257 depends on whether the altered water supply is sufficient to meet their demand, which itself
258 could be evolving³⁷. Considering that water stress, owing to the insufficient water supply to
259 meet the demand, is the primary factor limiting dryland vegetation growth, the outcome of
260 vegetation changes provides a useful surrogate metric for evaluating ongoing water stress of
261 dryland vegetation.

262 Vegetation greenness indices from satellite observations (for example the Leaf Area Index, LAI;
263 Normalized Difference Vegetation Index, NDVI) consistently show a significant positive trend
264 in dryland foliage cover since the 1980s²⁸⁻³⁰, co-occurring with the enhanced atmospheric
265 aridity indicated by VPD and AI. This enhanced dryland vegetation growth has remained strong
266 into the 21st century, as confirmed by greenness indices from the well-calibrated MODIS
267 collection 6 (**Fig. 2e**) and SPOT satellite data^{32,73}. Some regional hotspots of vegetation
268 greening also overlap with drylands under intensive agricultural expansion, such as in India,
269 the North China Plain, the U.S. Great Plains and southeast Australia^{32,73}.

270 Furthermore, aboveground production of dryland ecosystems, based on both empirical
271 observation-based product and process-based models, also presents an increasing trend that
272 accounts for over 50% of the increase in global carbon sink during 1982-2011 (ref. ⁶) (**Fig. 2e,**

273 **Table 1).** Dryland gross primary production (GPP) simulated by DGVMs and ESMS also
274 increases at a rate of 0.6 PgC decade⁻¹ and 1.0 PgC decade⁻¹, respectively. Such changes
275 correspond to an overall reduction in the areal coverage of vegetation growth-defined drylands
276 (f_{veg}) by 4.8% (for DGVMs) and 5.5% (for ESMS) over 1948-2005 (**Figs. 2j, Table 1**), in
277 contrast to the areal increases implied by f_{VPD} and f_{AI} .

278 Thus, a holistic overview of changes in surface aridity and dryland extent suggests that aridity
279 changes involve multi-dimensional land surface responses to climate change, which could not
280 be captured by any single offline aridity metric. This fact is particularly critical for dryland
281 assessment, as different indices point to highly divergent aridity changes and rates of dryland
282 expansion in recent decades. Specifically, dryland soil moisture and surface runoff decrease
283 following near-surface atmospheric drying (based on VPD), albeit with substantial uncertainties
284 and regional heterogeneity. In contrast, satellite records and models consistently illustrate a
285 greening and more productive trend in the warmer and CO₂-enriched drylands.

286

287 **[H1] Future aridity changes in drylands**

288 With atmospheric and land surface drying observed since around the 1950s, there is clear
289 interest in understanding how dryland aridity conditions will change with future warming.
290 Indeed, given that water resource shortage is the major constraint to socioeconomic growth and
291 ecological security in drylands, understanding future aridity changes is critical to regionally
292 targeted adaptation planning and decision making^{17,41}. ESMS provide sufficient climate and
293 land surface diagnostics to allow for systematic assessment of future aridity metrics, and have

294 been widely tested and used^{10,17,24,40,63}. To better understand dryland projections under various
295 temperature thresholds, we quantify the percentage change in dryland area for different aridity
296 metrics (f_{atm} , f_{AI} , f_{soil} , f_{hyd} and f_{veg}) in different regions using CMIP5 ESM projections (**Fig. 3**).

297

298 **[H2] CMIP5-projected changes**

299 AI-based aridity projections with CMIP5 models estimate a persistent increase of global
300 dryland extent by ~1-4% depending on temperature threshold used (**Figs. 2g, 3f**). These changes
301 are broadly consistent with previous analyses which suggest a 4% and 10% increase of global
302 dryland extent by 2100 relative to 1961-1990 under RCP4.5 (an intermediate emission scenario)
303 and RCP8.5 (a high-end emission scenario), respectively²⁴. Indeed, when anthropogenic
304 warming is over 1.5°C above pre-industrial, the signal of increased aridity can be distinguished
305 from natural variability for 8% and 24% of the global land surface for the two scenarios; for
306 2°C warming, these values increase to 10% for RCP4.5 and 32% for RCP8.5 (ref. ¹⁷). However,
307 this expansion is not spatially uniform; for example, up to 10% increases in dryland extent are
308 projected for southern Africa with 2°C warming, whereas a reduction of ~2% is anticipated for
309 northern Africa (**Fig. 3f**).

310 Global drylands are commonly divided into four subcategories (hyper-arid, arid, semi-arid and
311 dry sub-humid) based on a range of AI thresholds¹⁰ (**Box 1**). Among these four subcategories,
312 semi-arid and arid regions are estimated to expand in area by 1-15% and 1-5%, respectively,
313 under 2°C warming (**Fig. 3g-j**). The expansion of semi-arid regions mainly occurs in the
314 Mediterranean, southern Africa and North and South Americas, while the expansion of arid

315 regions occurs in southwestern Africa²⁴, predominately by encroaching into neighbouring less
316 arid zones (**Fig. 3g-j**). The spatial extent of dry sub-humid regions, in contrast, is projected to
317 slightly decrease through fast converting to drier climates (**Fig. 3g**). When accounting for CO₂
318 impacts on surface hydraulic resistance in the definition of AI ($f_{AI_CO_2}$), a qualitatively similar
319 expansion of global drylands is found, although the expansion rate is lower for almost all the
320 continents (**Fig. 3f**), as also evident in the present climate.

321 For alternative interpretations of dryland extent, projected changes generally exhibit similarities
322 in sign to those found for the historical period. Specifically, under RCP4.5, ESMs project that
323 historical trends of strongly increasing f_{atm} , slightly increasing f_{soil} , and strongly decreasing f_{veg}
324 will continue to the end of the 21st century (**Fig. 2**). In more detail, f_{atm} is anticipated to
325 experience rapid expansion across all the continents, exceeding 10% of total area when
326 warming is higher than 2°C (**Fig. 3a**). This widespread atmospheric drying trend is also
327 evidenced by the progressive expansion of more arid dryland subcategories into previously less
328 arid regions (**Fig. 3b-e**). Similarly, f_{soil} is also projected to increase throughout the 21st century
329 across all the continents except for northern Africa (**Fig. 3k**), with the largest fractional increase
330 occurring in semi-arid regions (**Fig. 3l-o**). One notable change is that although f_{hyd} historically
331 shows a slight increasing trend, this metric is projected to be reversed to a future decreasing
332 trend under RCP4.5 (**Fig. 2i, Table 1**). However, the projected future f_{hyd} change is regionally
333 heterogeneous, with slight expansions anticipated in North America, South America and
334 southern Africa, but slight reductions in Eurasia, Australia and northern Africa (**Fig. 3p**).

335 Following a similar trajectory to historical changes, the projected future f_{veg} shows a widespread
336 and persistent decreasing trend (**Figs. 2j, 3u**), spanning from -6.6% in southern Africa to -25.3%

338 $\pm 3.3\%$ globally relative to the 1961-
339 1990 baseline (**Fig. 3u**). Vegetation in many of the historical transitional zones between dry
340 and wet climates (defined as sub-humid or semi-arid), such as in temperate central North
341 America and northeastern China, is expected to move from arid-climate-adapted to humid-
342 climate-adapted (**Fig. 3z**). All the four subcategories of dryland vegetation are expected to
343 decrease in area, except for semi-arid regions in Australia and Eurasia where more arid areas
344 are moving into this vegetation-defined semi-arid subcategory than those moving out of semi-
345 arid areas to dry sub-humid due to the stronger greening trend in arid ecosystems (**Fig 3v-y**).

346

347 **[H2] CMIP6-projected changes**

348 Adding to the well-established CMIP5 ensembles of simulations, newer simulations archived
349 in the Phase 6 of the Coupled Model Intercomparison Project (CMIP6)⁷⁴ offer higher spatial
350 resolution, improved physical parameterisations and the inclusion of additional Earth system
351 processes^{74,75}.

352 Under SSP2-RCP4.5 – a scenario of intermediate emission and continuing historical socio-
353 economic activities – CMIP6 ESMs project a persistent expansion of AI-based drylands over
354 the 21st century at an average rate of $0.28 \pm 0.02\%$ decade⁻¹ ($p < 0.05$) driven by a positive VPD
355 trend of 0.030 ± 0.001 kPa decade⁻¹ (**Supplementary Table 5; Supplementary Fig. 5**). Owing
356 to the greater growth of atmospheric CO₂ forcing in SSP2-RCP4.5, this rate of dryland
357 expansion is larger than the $0.20 \pm 0.02\%$ decade⁻¹ ($p < 0.01$) projected by CMIP5 under RCP4.5

358 (Table 1).

359 When examining hydrological changes, CMIP6 ESMs show a significant increase in both total-
360 column soil moisture and surface runoff over 2015-2100: $0.05 \pm 0.01\%$ decade⁻¹ ($p < 0.01$) and
361 0.03 ± 0.01 mm yr⁻¹ ($p < 0.01$), respectively (Supplementary Fig. 5c, d). Despite the overall
362 surface wetting, changes are spatially heterogeneous and regional hotspots of strong drying
363 occur in the Mediterranean, western North America, southern Africa and Australia⁶⁰. The
364 overall wetting projected by CMIP6 ESMs is in contrast to the overall drying (or insignificant
365 change) projected by CMIP5 (Fig. 2c, d), which might be attributed to precipitation
366 enhancements in the Middle East and northern Africa⁶⁰ and higher surface resistance under
367 elevated CO₂ (ref⁴⁵) in the former. A caveat is that such CO₂ regulation of hydrological
368 dynamics has not been explicitly considered in some CMIP models because they represent a
369 class of Atmosphere-Ocean General Circulation Model (AOGCM) without simulating dynamic
370 vegetation. Hence, uncertainties exist in previous CMIP-based assessments of future
371 hydrological changes as AOGCMs are commonly included^{45,60,63}. For dryland ecosystem
372 responses, CMIP6 ESMs also project that the historical trends of ecosystem greening and
373 enhanced productivity will continue into the near future, similar to CMIP5 ESMs.

374 Model projections from CMIP5 therefore broadly show a persistence of contemporary trends
375 of dryland aridity changes throughout the 21st century. In particular, despite the continuously
376 rising atmospheric dryness and soil moisture stress, dryland ecosystems are expected to
377 continue greening. The divergent aridity changes over drylands with CMIP5 ESMs are also
378 predicted by recently released CMIP6 simulations; however, these project a stronger
379 atmospheric drying based on VPD and AI, and a robust trend of land surface wetting (rather

380 than drying or slight wetting based on CMIP5) assessed with soil moisture and runoff.

381

382 **[H1] Mechanisms for dryland aridity changes**

383 It is generally known that many land and atmospheric aridity processes, such as VPD, soil
384 moisture and vegetation greenness, are essentially coupled over sub-seasonal to inter-annual
385 timescales^{47,48,76} (**Fig. 4a**). However, over multi-decadal or longer timescales, highly
386 divergent—and in some instances decoupled—trends of dryland aridity changes emerge, the
387 size and direction of which are dependent on the chosen aridity metric. Specifically, as
388 discussed, atmospheric aridity, characterised by water vapour and precipitation deficits, does
389 not fully propagate to water deficits in the hydrosphere and the biosphere. This phenomenon is
390 likely because each component of the coupled atmosphere-plant-hydrology system has a
391 distinct and interactive response to rising atmospheric CO₂ and associated effects (**Fig. 4a**), and
392 thus reveals different aspects of dryland aridity changes. In particular, accounting for the soil
393 moisture constraints and leaf stomatal physiological response to rising CO₂ helps explain and
394 reconcile the divergence in aridity changes by different metrics to some extent, as now
395 discussed.

396

397 **[H2] Thermodynamic changes drive higher atmospheric demand for water**

398 Observed atmospheric drying – that is, rising VPD (**Fig. 2a,f**) – is generally accepted as a simple
399 thermodynamic consequence of warming^{18,36}. The lack of surface moisture and evaporative
400 cooling amplifies regional surface warming in drylands compared to humid lands and oceans².

401 The higher temperatures augment the capacity of the air to hold more water vapour. However,
402 the greater warming over land than oceans impedes the transport of moist air masses from
403 oceans to the land, particularly in subtropical subsidence zones, making the increase of near-
404 surface specific humidity over the land relatively small and insufficient to follow Clausius-
405 Clapeyron scaling ($\sim 7\% \text{ } ^\circ\text{C}$)^{18,77,78}. The enlarged contrast between actual and saturated water
406 vapour, that is, higher VPD, provides an explanation for the PET increase^{18,24,36}, which exceeds
407 concurrent precipitation increases and thus causes reduced AI values (enhanced aridity) and the
408 associated expansion of dryland extent^{10,18,24,25} (**Figs. 2b, 2g, 3f**).

409 Furthermore, land surface processes also modulate atmospheric dryness through land-
410 atmospheric feedbacks^{48,76} (**Fig. 4a**). For instance, warming-induced depletion of soil moisture
411 attenuates evaporative cooling and elevates temperature (thus also elevating VPD and PET),
412 while simultaneously enhancing atmospheric stability and inhibiting cloud formation and
413 precipitation generation⁷⁶. Soil moisture depletion also strengthens the gradients of air humidity
414 and pressure between drylands and surrounding humid regions, which promotes low-level
415 moisture convergence and increases precipitation transported to global drylands⁷⁹. Jointly, these
416 compensatory physical processes lead to an exacerbation of surface aridity characterized by
417 decreased AI values⁷⁶.

418 Importantly, the explanation of dryland aridity changes with atmospheric thermodynamics and
419 regional land-atmosphere interactions does not account for structural changes of large-scale
420 atmospheric circulations. In particular, the Hadley Circulation is essential for the development
421 of subtropical dryland climates². Observational evidence has indicated a widening (or poleward
422 expansion) of the subsiding branches of the Hadley Circulation, as well as a strengthening of

423 descending motion in the subtropics^{80,81}. These circulation changes suppress convective
424 precipitation and reduce tropospheric humidity, hence intensifying surface aridity in subtropical
425 zones^{80,81}. However, uncertainties remain in changes of the Hadley Circulation and associated
426 climatic consequences, and they are not able to explain the observed overall increase in
427 precipitation over subtropical lands². In addition, climate model projections of drier subtropics
428 under future warmer climates contradict paleoclimatic evidence of wetter subtropics in past
429 warm periods⁸²; the wetter subtropics under past warm climates are suggested to co-occur with
430 weakened (rather than present-day strengthened) subtropical subsidence of the Hadley
431 circulation associated with weaker-than-present meridional sea-surface temperature gradients⁸².

432

433 **[H2] Vegetation physiological responses to rising atmospheric CO₂**

434 Assuming fixed or only small increases in precipitation, alongside no change in direct human
435 consumption, available water resources (soil moisture and runoff) over the land will decrease.
436 This reduction arises from anthropogenic warming-enhanced evaporative losses owing to
437 heightened PET^{18,68,72,83}. However, changes in actual evapotranspiration (AET) are governed
438 by more than the thermodynamics which determine PET. In particular, the thermodynamically
439 driven growth in PET cannot translate into similar growth in AET over drylands, as the limited
440 soil moisture supply strongly constrains the AET increase if precipitation remains steady^{84,85}
441 **(Fig. 4b)**. There is also growing evidence that vegetation physiological processes have a critical
442 role in controlling AET and thus other hydrological fluxes^{45,86-89}. The different governing
443 processes of PET and AET create a growing gap between them under rising atmospheric CO₂,
444 which underlies the inconsistent changes between AI (depending on PET changes) and other

445 ecohydrological aridity measures (affected by AET by varying amounts) (**Fig. 4b**).

446 As atmospheric CO₂ increases, plant leaves partially close their stomata and reduce the amount
447 of water loss through stomatal transpiration. This leaf-scale stomatal regulation is simultaneous
448 with, and could be potentially counteracted by, changes in structural and functional attributes
449 of plants, including enhanced photosynthesis⁹⁰, increased canopy leaf area³² and deepened
450 rooting system⁹¹ (**Fig. 4a**). In particular, the expansion of foliage area induces extra water loss
451 via leaf transpiration and canopy evaporation of intercepted rainfall, while simultaneously
452 decreasing evaporative water loss from the soil surface^{32,92}. As plant transpiration accounts for
453 more than half of the land AET in dryland natural ecosystems⁹³, transpiration (rather than
454 evaporation) responses to higher CO₂ will likely dominate the overall dryland AET changes in
455 a CO₂-enriched world⁹⁴.

456 However, at least for the recent past (1948-2016), there is no consensus as to the net
457 hydrological effect of plant physiological responses to higher CO₂, linked to uncertainties in
458 the complex interactions and compensations among relevant biophysical processes^{19,95}. Under
459 future scenarios with a much higher atmospheric CO₂ concentration (for instance, reaching a
460 quadrupling of the pre-industrial CO₂ level), model projections generally agree on a net
461 decrease of canopy-level transpiration and land AET after accounting for both stomatal
462 regulation and foliage expansion^{45,86,87,89}. This physiological forcing of high atmospheric CO₂
463 on AET could even dominate over its radiative forcing in some less-arid dryland areas with
464 sizable vegetation cover⁸⁷.

465

466 The plant physiological responses to elevated CO₂ can partly explain the divergent dryland
467 aridity changes, simultaneously ameliorating ecohydrological water stress and increasing
468 atmospheric dryness (**Supplementary Figure 6**). The stomatal regulation of transpiration under
469 elevated CO₂ level can conserve water, which generally favors the partitioning of precipitation
470 towards runoff and soil moisture^{45,86-88,94,96} (**Figs. 4, Supplementary Figure 6**). Vegetation
471 growth of water-limited biomes, as for drylands, is more sensitive to soil moisture deficit than
472 to atmospheric moisture deficit^{97,98}, and hence CO₂-driven water saving can offset the higher
473 water demand driven by a warmer atmosphere. Such CO₂-driven water-saving is sufficient to
474 ameliorate water limitations for photosynthesis in semi-arid grasslands, as confirmed by
475 manipulative free-air CO₂-enrichment experiments⁹⁹⁻¹⁰¹ and factorial simulations with DGVMs
476 (**Box 2**). This water-saving mechanism, in concert with CO₂-induced stimulation of
477 photosynthesis, longer growing seasons and attenuated soil moisture stress at places with
478 increased precipitation, translates to extra carbon gain and enhanced growth and moves the
479 dryland ecosystem to a new hydro-ecological equilibrium^{28,102,103}.

480 Meanwhile, the physiologically induced transpiration decrease also feeds back to surface
481 climate through reduced evaporative cooling, thus contributing to the warming¹⁰⁴ and relative
482 drying of the near-surface air, which is reflected in enhanced VPD^{76,89} (**Supplementary Figure**
483 **6**). The CO₂ physiological effect on hydrology and surface climate, as previously discussed, is
484 small in extremely arid areas, but in semi-arid and sub-humid areas, this effect is substantially
485 larger and even comparable to that in humid areas (**Supplementary Figure 6**).

486

487 **[H2] Uncertainties in current understanding of CO₂ physiological impacts**

488 Large uncertainties exist in the estimation of CO₂ physiological impacts on dryland
489 ecohydrological changes. Many studies of CO₂ physiological forcing are based only on
490 numerical simulations that depend heavily on model parameterisation schemes of ecosystem
491 response^{45,86-89,105}. For example, some experimental studies suggest that the capacity of dryland
492 plants to optimize their carbon sequestration and water utilization under higher CO₂ is limited
493 owing to the dominant role of soil moisture limitations in controlling plant physiological
494 responses to CO₂ (refs. ^{106,107}) and possible nutrient depletion¹⁰⁸. Such processes are not yet
495 sufficiently understood, and consequently errors in their parameterisation in DGVMs might be
496 substantial³². At present, more observational and experimental techniques, such as leaf gas
497 exchange, stable isotope discrimination and eddy covariance measurement, are now
498 implemented to investigate plant water use¹⁰⁹⁻¹¹¹. Yet, these approaches are rarely applied to the
499 scale of ecosystem or river basin, due to the substantial discrepancy at different spatial and
500 temporal scales¹⁰⁹ or the short temporal coverage that precludes the detection of slowly
501 evolving CO₂ impacts.

502 ESMS project that dryland vegetation greening will continue to benefit from future atmospheric
503 CO₂ enrichment (refs. ^{32,103}). However, as temperature continues to increase, whether the
504 positive CO₂ physiological impact on vegetation will persist remains an open question.
505 Temperature and precipitation feedbacks from CO₂-induced stomatal closure and AET
506 reduction can amplify the risk of surface heat stress¹¹²⁻¹¹⁴, which might offset, or even reverse,
507 the positive effect of water stress relief. More importantly, with increasing warming, plants
508 could need to keep stomata open to cool their leaves from irreversible heat damage, despite
509 elevated CO₂ allowing for reduced stomatal aperture to maintain the same or even raised

510 photosynthetic rate^{115,116}. This required stomatal opening could be increasingly important for
511 dryland biomes as temperatures rise, since current temperatures appear to be near or above the
512 optimum for photosynthesis¹¹⁷. Future research needs to place more emphasis on understanding
513 possible nonlinearities or tipping points of critical transitions^{50,51} in dryland ecosystem
514 responses to future global warming, and improving their representations in process-based
515 models. In particular, long-term manipulative field experiments will be useful to better
516 characterise any nonlinear features of plant responses and assess dangerous levels of future
517 warming over drylands^{118,119}.

518

519 **[H1] Towards a human-dominated dryland**

520 Earth is now in the Anthropocene era¹²⁰ when humans are playing a central or even dominant
521 role in shaping terrestrial greenness patterns and modifying regional hydrological cycles^{62,121-}
522 ¹²³. Direct human impacts are, in some instances, more substantial than natural factors and
523 indirect human forcing via climate change. Global drylands are currently experiencing the
524 fastest population growth in the world¹²⁴, which makes the already fragile dryland environment
525 even more vulnerable to water scarcity. Therefore, human freshwater use, which is heavily
526 influenced by demographical, social, economic and technological factors¹²⁵, must be
527 incorporated in dryland aridity assessment and predictions. Global hydrological models
528 (GHMs), forced by varying scenarios of both historical and future socio-economic factors and
529 greenhouse-gas emissions (**Supplementary Methods**), are available for such assessments^{126,127}
530 (**Fig. 5**).

531 GHMs indicate that since the 1950s, rapid population growth and economic development has
532 increased human water demand in drylands by approximately 200% (**Fig. 5g**). Furthermore,
533 this rapid increase in human water demand is expected to increase by ~270% (on the baseline
534 of 1950s) by 2090s under SSP2-RCP6.0, a no-mitigation emission pathway (**Fig. 5g**).
535 Agricultural irrigation contributes the greatest overall increase of dryland water use for all the
536 continents, for both historical and future periods^{128,129} (**Fig. 5**). In addition, industrial and
537 domestic water demands are also projected to increase substantially, especially in African
538 drylands (**Fig. 5b, e**).

539 However, GHMs forced with changing socio-economic factors do not project monotonically
540 increasing human water demand throughout the 21st Century (**Fig. 5g**). These models estimate
541 an increase in water demand consistently for all the continents before the 2030s. After the
542 2030s, however, regional projections diverge, with a continuous rise in Africa (**Fig. 5b, e**), a
543 levelling off in Eurasia and South America (**Fig. 5c, d**) and a decline in North America and
544 Australia (**Fig. 5a, f**). Given the relatively small water supply changes of surface runoff, the
545 rapid augmentation of water needs in Eurasia, South America and in particular Africa will
546 exacerbate societal water scarcity (the gap between water demand and supply) in those regions
547 (**Fig. 5**). This geographical divergence also highlights a major concern that many of the poorest
548 regions, with very limited access to financial and technological resources, are more likely to be
549 exposed to high pressures of water scarcity in the future. Importantly, there is accumulating
550 experimental evidence that crop plants can use water more efficiently under rising atmospheric
551 CO₂ (refs. ¹³⁰⁻¹³²). The CO₂ physiological effects can partly, though not fully, offset the
552 anticipated increase of agricultural water consumption, and thus alleviate the adverse impact of

553 surface warming and drying to some extent¹³⁰⁻¹³².

554 The rapidly growing freshwater demands might not be sustainable, and have already imprinted
555 noticeable footprints on local to global hydrological cycles. Agricultural expansion and
556 intensification, though contributing to regional greening and increased vegetation productivity
557 in many places^{32,73}, are often accompanied with excessive withdrawal of surface waters (mainly
558 runoff) and over-extraction of groundwater storage^{128,133,134}. In particular, gravity-based remote
559 sensing demonstrates that groundwater levels in India¹³⁵, the North China Plain¹³⁶ and western
560 U.S.⁸³ are falling at an alarming rate. Groundwater extraction for agricultural irrigation is now
561 exceeding the natural recharge rate in these regions, recognised as the main cause for the
562 observed decline in groundwater levels^{128,134,135}. Many plant species in arid and semi-arid areas
563 depend on shallow groundwater for survival, particularly during dry seasons when other water
564 sources are largely unavailable^{137,138}. Therefore, such unsustainable groundwater depletion also
565 poses a significant threat to the health of dryland natural ecosystems^{138,139}.

566 In addition to the direct extraction of water resources, other human land-use management
567 practices, such as afforestation (or reforestation), deforestation, overgrazing and urbanization,
568 also leave remarkable imprints on dryland ecohydrological systems. For example, while
569 contributing to halting desertification and increasing carbon storage^{140,141}, large-scale
570 ecological restoration programmes implemented in semi-arid or sub-humid North and West
571 China have caused extra evaporative water loss and a related significant decrease in regional
572 runoff and terrestrial water storage^{140,142,143}. The faster return of water to the atmosphere means
573 that less water is available for other socio-economic needs. Meanwhile, overgrazing is also a
574 significant anthropogenic factor contributing to grassland deterioration and even the shift of

575 dominant vegetation types, potentially disturbing local hydrological cycles. This deterioration
576 is a key environmental problem faced by regions economically dependent on livestock, such as
577 Mongolia, central Eurasia, Latin America and and Sub-Saharan Africa^{144,145}. By removing
578 protective plant cover and by livestock trampling, overgrazing may cause the compaction of
579 soils, reducing infiltration and accelerating runoff and soil erosion¹⁴⁶.

580 More efficient water-resource management measures can help to cope with the increasing water
581 crisis, with substantial co-benefits for the sustainability of the coupled dryland social-ecological
582 system. First, taking advantage of the increasing crop water-use efficiency under elevated CO₂
583 (refs. ^{131,132}), it might be possible to gradually reduce irrigation water usage per unit area of
584 agricultural land. This irrigation reduction is complementary to other agricultural water
585 management approaches, such as rainwater harvesting, precise irrigation, improved irrigation
586 infrastructure. Second, there is growing attention placed on the benefits of future forestry
587 practices, and especially afforestation as a potential solution to partially offset CO₂
588 emissions^{147,148}. Afforestation programmes in dryland regions need to use locally adapted and
589 water-efficient indigenous species to avoid unnecessary evaporative water losses¹⁴⁹. Careful
590 evaluation is also required of the land carrying capacity to support anticipated plant
591 growth^{140,150}. Third, policy decisions may gain from incorporating water-relevant ecological
592 information from the ever-expanding near real-time data streams from space. For example, the
593 incorporation of satellite-monitoring of GPP and chlorophyll fluorescence into drought early-
594 warning systems¹⁵¹ can help guide governments to take anticipatory mitigation actions in
595 preserving farming livelihoods and food security.

596 New water-conservation technologies are also helpful to safeguard dryland water and food

597 security. For example, improved agricultural biotechnology is expected to breed more drought
598 and/or salt-tolerant, water-efficient and more productive cereal and forage crops¹⁵². Such
599 advances will simultaneously increase agricultural production and reduce water usage.
600 Modelling evidence also suggests that the adoption of new technologies, such as developing
601 renewable energy and recirculating dry-cooling systems in electricity generation, could lower
602 ~32% of global water requirements by 2100 under the SSP5 scenario (ref. ¹⁵³). Nonetheless, the
603 effectiveness of such technological innovations for drylands depends on their transfer to and
604 implementation by some of the world's poorest countries.

605

606 **[H1] Summary and future perspectives**

607 Dryland ecosystems are a pivotal part of the Earth system and their sustainability is critical both
608 locally and for our shared societal future. While water is the central component in defining
609 dryland social-ecological systems, aridity in drylands is tightly interconnected with climate,
610 vegetation and humans, all of which are vary over different spatio-temporal scales. Whilst
611 numerous studies define dryland changes with a broad range of metrics, these often generate
612 highly conflicting conclusions. Such discrepancies lead to less trust in projections of
613 environmental change and can preclude the accurate determination of dangerous thresholds of
614 climate alteration.

615 This review leverages comprehensive strands of data and research pertaining to drylands for a
616 holistic overview of their global changes. By viewing the emerging aridity changes as adjusting
617 attributes of a coupled atmosphere-ecohydrology-human system, we provide a cohesive picture

618 of recent, ongoing and future dryland changes (**Fig. 6**). At short timescales such as daily to
619 inter-annual, aridity changes are primarily governed by climate variability regardless of the
620 metric used. Yet, over longer decade-to-century timescales, the CO₂ physiological effect is
621 likely a more important driver for vegetation-related aridity changes, with important feedbacks
622 to local and regional hydrological cycles (**Fig. 6**). The role of plant physiological mechanisms
623 in ameliorating plant water stress and fostering plant growth will become even more important
624 and helpful, against a backdrop of rising water and food demands by the rapidly growing
625 population (**Fig. 6**).

626 Although the mechanistic understanding of surface aridity changes is for the recent past and the
627 near future, it might also have broader implications beyond the contemporary timescale. In
628 particular, the CO₂ physiological forcing provides a useful mechanism for explaining the
629 warmer-and-greener association observed over the geological timescale. Ice-core and pollen-
630 based hydroclimate reconstructions suggest that warmer inter-glacial periods (for example, the
631 Pliocene period with atmospheric CO₂ concentration of 350–450 ppm, as comparable to the
632 current CO₂ level) are often associated with lower dust levels (often indicative of a wetter land
633 surface)¹⁵⁴ and generally higher vegetation cover, compared to colder glacial periods (for
634 example, the Last Glacial Maximum with atmospheric CO₂ concentration of ~190 ppm)¹⁵⁵⁻¹⁵⁷.
635 This phenomenon again contradicts with model-estimated lower AI values (land surface drying)
636 for warmer periods¹⁵⁸, but does agree with present-day trends for increasing vegetation cover.
637 That is, analysis from the current climate suggesting that the physiological influence of higher
638 CO₂ levels in warmer periods shapes the surface water cycle and prevents the expansion of arid
639 and semi-arid ecosystems, and this present-day process has presumably operated throughout

640 the geological timescale. Decreased dust deposition in warmer periods does not, however,
641 necessarily imply a wetter land surface owing to potential confounding factors such as changes
642 in large-scale circulation patterns⁸², wind speed, aerosol concentrations, and the likelihood that
643 less dusty air is itself a result of higher vegetation cover^{63,154}.

644 Looking forward, we identify several remaining knowledge gaps as priorities for future research
645 and policy decisions. Aridity, calculated as a long-term but changing average state of water
646 scarcity, cannot represent all aspects of the societally relevant hydrological responses expected
647 for future climatic states. Future research needs to prioritize the understanding of possible
648 enhanced risk posed by short-term hydro-climatic anomalies and how ecosystems subsequently
649 respond and adapt to such climate perturbations.

650 As the climate gets warmer, there is substantial evidence of increasing chances of more frequent
651 and severe climate extremes, particularly droughts^{107,159-161}. Extreme dry events can trigger
652 detrimental damage to the fragile dryland ecosystems, including raised mortality levels and
653 enhanced fire risks¹⁶²⁻¹⁶⁴. As one of the most fire-prone ecosystems, drylands account for more
654 than 80% of global wildfires, with massive losses of plant biomass and soil nutrients^{165,166}.

655 Observational evidence shows widespread woody encroachment in subtropical savannas
656 associated with decreased burned areas and fire return intervals during 1997-2016 (ref. ¹⁶⁷).

657 Contrary to the observed downward trends of historical records, current fire models usually
658 project rising risks of fire disturbances under future climate change, yet with a large spread of
659 probabilities^{166,168}. The impact of future shifting fire regimes on dryland ecosystem-hydrology
660 changes is thus still largely uncertain. However, dryland vegetation is also highly resilient and
661 can often recover quickly from past disturbances¹⁶⁹, despite possible increasing risks from

662 droughts and fires. The high resilience and fast recovery might represent a key mechanism for
663 the adaptation of dryland vegetation to past and future climate change, and can additionally
664 contribute to the differences noted between changes of vegetation aridity and those of other
665 aridity indicators.

666 Global drylands also encompass a diverse range of regions, cultures and ecosystems, resulting
667 in regional divergence in their aridity changes and associated impacts. This divergence implies
668 highly regionalised challenges in meeting the societal and ecosystem needs of water resources³.
669 Targeted regional assessments of dryland aridity changes will better inform effective mitigation
670 actions if tailored to different specific localised needs.

671 There additionally remain challenges to observe and model accurately long-term changes of
672 surface aridity and water resources^{159,170,171}. Field measurements and experiments remain scarce
673 in drylands, and at present, datasets are often too short to provide definitive answers on the
674 long-term effects of CO₂-fertilization and stomatal behaviour. The scarcity of data prevents
675 characterising any potential nonlinear responses as atmospheric CO₂ concentrations rise even
676 higher. Thus, there is a pressing need for future efforts to build more extensive and high-quality
677 dryland observation networks that operate over a range of spatial scales and substantial periods
678 of time. Yet, even for measurements that are available, there need to be more far-reaching
679 integrated analyses of emerging space and ground-based measurements, such as eddy
680 covariance, FACE experiments, plant functional traits and tree-ring chronologies, to provide a
681 more complete mechanistic understanding of ongoing land surface processes. Moreover, future
682 hydrological models must treat vegetation as a dynamic component, and explicitly consider the
683 feedbacks of its structural and physiological changes to other key water-cycle components.

684 Current models generate substantial uncertainties in projected trajectories of dryland water-
685 resource availability and requirements. Constraining such uncertainties requires refining the
686 representation of the complex interactions between the climate, hydrology, ecosystems and
687 humans. An improved predictive capability will support policymaking to achieve sustainable
688 management of global drylands, to better service different societal and ecosystem needs in a
689 warmer and CO₂-enriched world.

690 **References**

- 691 1 Reynolds, J. F. *et al.* Global desertification: building a science for dryland development.
692 *Science* **316**, 847-851 (2007).
- 693 2 Huang, J. *et al.* Dryland climate change: recent progress and challenges. *Rev. Geophys.*
694 **55**, 719-778 (2017).
- 695 3 IPCC. *Climate Change and Land: an IPCC Special Report on Climate Change,*
696 *Desertification, Land Degradation, Sustainable Land Management, Food Security, and*
697 *Greenhouse Gas Fluxes in Terrestrial Ecosystems* (eds Akhtar-Schuster, M., Driouech,
698 F. & Sankaran, M.) Ch. 3 (IPCC, Cambridge Univ. Press, 2019).
- 699 4 Prävălie, R. Drylands extent and environmental issues. A global approach. *Earth-Science*
700 *Rev.* **161**, 259-278 (2016).
- 701 5 D’Odorico, P., Bhattachan, A., Davis, K. F., Ravi, S. & Runyan, C. W. Global
702 desertification: drivers and feedbacks. *Adv. Water Resour.* **51**, 326-344 (2013).
- 703 6 Ahlström, A. *et al.* The dominant role of semi-arid ecosystems in the trend and variability
704 of the land CO₂ sink. *Science* **348**, 895-899 (2015).
- 705 **Highlights the critical role of drylands in the global carbon budget by**
706 **demonstrating that semi-arid ecosystems dominate the interannual variability**
707 **and the increasing trend of global terrestrial carbon sink.**
- 708 7 Maestre, F. T. *et al.* Plant species richness and ecosystem multifunctionality in global
709 drylands. *Science* **335**, 214-218 (2012).
- 710 8 Millennium Ecosystem Assessment. *Ecosystems and Human Well-Being: Desertification*
711 *Synthesis* (World Resources Institute, Washington DC, 2005).
- 712 9 El-Beltagy, A. & Madkour, M. Impact of climate change on arid lands agriculture. *Agric.*
713 *Food Secur.* **1**, 3 (2012).
- 714 10 Huang, J., Yu, H., Guan, X., Wang, G. & Guo, R. Accelerated dryland expansion under
715 climate change. *Nat. Clim. Change* **6**, 166-171 (2016).
- 716
- 717 11 Cook, K. H. & Vizy, E. K. Detection and analysis of an amplified warming of the Sahara
718 Desert. *J. Clim.* **28**, 6560-6580 (2015).
- 719 12 Zhou, L., Chen, H. & Dai, Y. Stronger warming amplification over drier ecoregions

- 720 observed since 1979. *Environ. Res. Lett.* **10**, 064012 (2015).
- 721 13 Fu, B. *et al.* The Global-DEP conceptual framework—research on dryland ecosystems to
722 promote sustainability. *Curr. Opin. Environ. Sustain.* **48**, 17-28 (2020).
- 723 **Proposes a conceptual framework that aims to facilitate actionable pathways**
724 **towards sustainable development of global dryland socio-ecological systems.**
- 725 14 Larigauderie, A. & Mooney, H. A. The Intergovernmental science-policy Platform on
726 Biodiversity and Ecosystem Services: moving a step closer to an IPCC-like mechanism
727 for biodiversity. *Curr. Opin. Environ. Sustain.* **2**, 9-14 (2010).
- 728 15 Convention on Biological Diversity, Aichi Biodiversity Targets. [http://www.cbd.](http://www.cbd.int/sp/targets/default.shtml)
729 [int/sp/targets/default.shtml](http://www.cbd.int/sp/targets/default.shtml).
- 730 16 United Nations. *Transforming Our World: The 2030 Agenda for Sustainable*
731 *Development* (United Nations General Assembly, New York, NY, 2015).
- 732 17 Park, C.-E. *et al.* Keeping global warming within 1.5 °C constrains emergence of
733 aridification. *Nat. Clim. Change* **8**, 70-74 (2018).
- 734 18 Sherwood, S. & Fu, Q. A drier future? *Science* **343**, 737-739 (2014).
- 735 19 Ukkola, A. M. *et al.* Reduced streamflow in water-stressed climates consistent with CO₂
736 effects on vegetation. *Nat. Clim. Change* **6**, 75-78 (2015).
- 737 20 Wang, J. *et al.* Recent global decline in endorheic basin water storages. *Nat. Geosci.* **11**,
738 926-932 (2018).
- 739 **Provides observational evidence for widespread loss of terrestrial water storage**
740 **over global endorheic basins during 2002-2016 from climate variability and human**
741 **water extractions.**
- 742 21 Scheff, J. & Frierson, D. M. W. Terrestrial aridity and its response to greenhouse warming
743 across CMIP5 climate models. *J. Clim.* **28**, 5583-5600 (2015).
- 744 22 Koutroulis, A. G. Dryland changes under different levels of global warming. *Sci. Total*
745 *Environ.* **655**, 482-511 (2019).
- 746 23 Schewe, J. *et al.* Multimodel assessment of water scarcity under climate change. *Proc.*
747 *Natl. Acad. Sci. USA* **111**, 3245-3250 (2014).
- 748 24 Feng, S. & Fu, Q. Expansion of global drylands under a warming climate. *Atmos. Chem.*
749 *Phys. Discuss.* **13**, 14637-14665 (2013).

- 750 25 Cook, B. I., Smerdon, J. E., Seager, R. & Coats, S. Global warming and 21st century
751 drying. *Clim. Dyn.* **43**, 2607-2627 (2014).
- 752 26 Zhang, P. *et al.* Abrupt shift to hotter and drier climate over inner East Asia beyond the
753 tipping point. *Science* **370**, 1095-1099 (2020).
- 754 27 He, B., Wang, S., Guo, L. & Wu, X. Aridity change and its correlation with greening over
755 drylands. *Agric. For. Meteorol.* **278**, 107663 (2019).
- 756 28 Donohue, R. J., Roderick, M. L., McVicar, T. R. & Farquhar, G. D. Impact of CO₂
757 fertilization on maximum foliage cover across the globe's warm, arid environments.
758 *Geophys. Res. Lett.* **40**, 3031-3035 (2013).
- 759 **Reveals widespread greening in global arid regions despite warming, and provides**
760 **quantitative theoretical evidence linking this greening pattern with elevated CO₂.**
- 761 29 Fensholt, R. *et al.* Greenness in semi-arid areas across the globe 1981–2007 — an Earth
762 Observing Satellite based analysis of trends and drivers. *Remote Sens. Environ.* **121**, 144-
763 158 (2012).
- 764 30 Andela, N., Liu, Y. Y., van Dijk, A. I. J. M., de Jeu, R. A. M. & McVicar, T. R. Global
765 changes in dryland vegetation dynamics (1988-2008) assessed by satellite remote
766 sensing: comparing a new passive microwave vegetation density record with reflective
767 greenness data. *Biogeosciences* **10**, 6657-6676 (2013).
- 768 31 Zhu, Z. *et al.* Greening of the Earth and its drivers. *Nat. Clim. Change* **6**, 791-795 (2016).
- 769 32 Piao, S. *et al.* Characteristics, drivers and feedbacks of global greening. *Nat. Rev. Earth*
770 *Environ.* **1**, 14-27 (2020).
- 771 33 Beck, H. E. *et al.* Global evaluation of four AVHRR–NDVI data sets: intercomparison
772 and assessment against Landsat imagery. *Remote Sens. Environ.* **115**, 2547-2563 (2011).
- 773 34 United Nations World Water Assessment Programme. *The United Nations World Water*
774 *Development Report: Water for a Sustain-able World* (UNESCO, 2015).
- 775 35 Wang, L. *et al.* Dryland ecohydrology and climate change: critical issues and technical
776 advances. *Hydrol. Earth Syst. Sci.* **16**, 2585-2603 (2012).
- 777 36 Roderick, M. L., Greve, P. & Farquhar, G. D. On the assessment of aridity with changes
778 in atmospheric CO₂. *Water Resour. Res.* **51**, 5450-5463 (2015).
- 779 **A comprehensive summary of contradictory viewpoints of “warmer is more arid”**

780 **versus “warmer is less arid” that arise from different interpretations of aridity**
781 **changes, and provides a roadmap for reconciling such disparities.**

782 37 Swann, A. L. S. Plants and drought in a changing climate. *Curr. Clim. Chang. Reports* **4**,
783 192-201 (2018).

784 38 Greve, P. *et al.* Global assessment of trends in wetting and drying over land. *Nat. Geosci.*
785 **7**, 716-721 (2014).

786 39 Smith, W. K. *et al.* Remote sensing of dryland ecosystem structure and function: progress,
787 challenges, and opportunities. *Remote Sens. Environ.* **233**, 111401 (2019).

788 40 Greve, P., Roderick, M. L., Ukkola, A. M. & Wada, Y. The Aridity Index under global
789 warming. *Environ. Res. Lett.* **14**, 124006 (2019).

790 41 Huang, J., Yu, H., Dai, A., Wei, Y. & Kang, L. Drylands face potential threat under 2°C
791 global warming target. *Nat. Clim. Change* **7**, 417-422 (2017).

792 42 Middleton, N. & Thomas, D. *World atlas of desertification*. (Arnold, 1997).

793 43 Fu, Q. & Feng, S. Responses of terrestrial aridity to global warming. *J. Geophys. Res.*
794 *Atmos.* **119**, 7863-7875 (2014).

795 44 Yang, Y. *et al.* Disconnection between trends of atmospheric drying and continental
796 runoff. *Water Resour. Res.* **54**, 4700-4713 (2018).

797 45 Yang, Y., Roderick, M. L., Zhang, S., McVicar, T. R. & Donohue, R. J. Hydrologic
798 implications of vegetation response to elevated CO₂ in climate projections. *Nat. Clim.*
799 *Change* **9**, 44-48 (2019).

800 46 Greve, P., Roderick, M. L. & Seneviratne, S. I. Simulated changes in aridity from the last
801 glacial maximum to 4xCO₂. *Environ. Res. Lett.* **12**, 114021 (2017).

802 47 Yuan, W. *et al.* Increased atmospheric vapor pressure deficit reduces global vegetation
803 growth. *Sci. Adv.* **5**, eaax1396 (2019).

804 48 Zhou, S. *et al.* Land-atmosphere feedbacks exacerbate concurrent soil drought and
805 atmospheric aridity. *Proc. Natl. Acad. Sci. USA* **116**, 18848-18853 (2019).

806 49 Grossiord, C. *et al.* Plant responses to rising vapor pressure deficit. *New Phytol.* **226**,
807 1550-1566 (2020).

808 50 Berdugo, M. *et al.* Global ecosystem thresholds driven by aridity. *Science* **367**, 787-790
809 (2020).

- 810 51 Keenan, T. F., Luo, X., Zhang, Y. & Zhou, S. Ecosystem aridity and atmospheric CO₂.
811 *Science* **368**, 251-252 (2020).
- 812 52 Yao, J. *et al.* Accelerated dryland expansion regulates future variability in dryland gross
813 primary production. *Nat. Commun.* **11**, 1665 (2020).
- 814 53 Trenberth, K. E. *et al.* Global warming and changes in drought. *Nat. Clim. Change* **4**, 17-
815 22 (2013).
- 816 54 Milly, P. C. D. & Dunne, K. A. Potential evapotranspiration and continental drying. *Nat.*
817 *Clim. Change* **6**, 946-949 (2016).
- 818 55 Milly, P. & Dunne, K. A. A hydrologic drying bias in water-resource impact analyses of
819 anthropogenic climate change. *J Am. Water Resour. As.* **53**, 822-838 (2017).
- 820 56 De Jeu, R. A. *et al.* Global soil moisture patterns observed by space borne microwave
821 radiometers and scatterometers. *Surv. Geophys.* **29**, 399-420 (2008).
- 822 57 Berg, A. & Sheffield, J. Climate change and drought: the soil moisture perspective. *Curr.*
823 *Clim. Chang. Reports* **4**, 180-191 (2018).
- 824 58 Feng, H. & Zhang, M. Global land moisture trends: drier in dry and wetter in wet over
825 land. *Sci. Rep.* **5**, 18018 (2015).
- 826 59 Berg, A., Sheffield, J. & Milly, P. C. D. Divergent surface and total soil moisture
827 projections under global warming. *Geophys. Res. Lett.* **44**, 236-244 (2017).
- 828 60 Cook, B. I. *et al.* Twenty-first Century drought projections in the CMIP6 forcing
829 scenarios. *Earth's Futur.* **8**, e2019EF001461 (2020).
- 830 61 Li, M., Wu, P., Ma, Z., Lv, M. & Yang, Q. Changes in soil moisture persistence in China
831 over the past 40 years under a warming climate. *J. Clim.* **33**, 9531-9550 (2020).
- 832 62 Rodell, M. *et al.* Emerging trends in global freshwater availability. *Nature* **557**, 651-659
833 (2018).
- 834 63 Dai, A., Zhao, T. & Chen, J. Climate change and drought: a precipitation and evaporation
835 perspective. *Curr. Clim. Chang. Reports* **4**, 301-312 (2018).
- 836 **Highlights the dominant role of CO₂ radiative forcing in shaping global land surface**
837 **drying patterns for the 21st Century.**
- 838 64 Schlaepfer, D. R. *et al.* Climate change reduces extent of temperate drylands and
839 intensifies drought in deep soils. *Nat. Commun.* **8**, 14196 (2017).

- 840 65 Li, L. *et al.* Global trends in water and sediment fluxes of the world's large rivers. *Sci.*
841 *Bull.* **65**, 62-69 (2019).
- 842 66 Yang, H. *et al.* Regional patterns of future runoff changes from Earth system models
843 constrained by observation. *Geophys. Res. Lett.* **44**, 5540-5549 (2017).
- 844 67 Wang, S. *et al.* Reduced sediment transport in the Yellow River due to anthropogenic
845 changes. *Nat. Geosci.* **9**, 38-41 (2015).
- 846 68 Milly, P. C. D. & Dunne, K. A. Colorado River flow dwindles as warming-driven loss of
847 reflective snow energizes evaporation. *Science* **367**, 1252-1255 (2020).
- 848 69 Trancoso, R., Larsen, J. R., McVicar, T. R., Phinn, S. R. & McAlpine, C. A. CO₂-
849 vegetation feedbacks and other climate changes implicated in reducing base flow.
850 *Geophys. Res. Lett.* **44**, 2310-2318 (2017).
- 851 70 Dai, A., Qian, T., Trenberth, K. E. & Milliman, J. D. Changes in continental freshwater
852 discharge from 1948 to 2004. *J. Clim.* **22**, 2773-2792 (2009).
- 853 71 Hobeichi, S., Abramowitz, G., Evans, J. & Beck, H. E. Linear Optimal Runoff Aggregate
854 (LORA): a global gridded synthesis runoff product. *Hydrol. Earth Syst. Sci.* **23**, 851-870
855 (2019).
- 856 72 Novick, K. A. *et al.* The increasing importance of atmospheric demand for ecosystem
857 water and carbon fluxes. *Nat. Clim. Change* **6**, 1023-1027 (2016).
- 858 73 Chen, C. *et al.* China and India lead in greening of the world through land-use
859 management. *Nat. Sustain.* **2**, 122-129 (2019).
- 860 74 Eyring, V. *et al.* Overview of the Coupled Model Intercomparison Project Phase 6
861 (CMIP6) experimental design and organization. *Geosci. Model Dev.* **9**, 1937-1958
862 (2016).
- 863 75 Eyring, V. *et al.* Taking climate model evaluation to the next level. *Nat. Clim. Change* **9**,
864 102-110 (2019).
- 865 76 Berg, A. *et al.* Land-atmosphere feedbacks amplify aridity increase over land under
866 global warming. *Nat. Clim. Change* **6**, 869-874 (2016).
- 867 **Reveals the important mechanism that declining soil moisture and altered**
868 **vegetation physiology under climate change and rising CO₂ could make the near-**
869 **surface even air warmer and drier.**

870 77 Stephens, C. M., McVicar, T. R., Johnson, F. M. & Marshall, L. A. Revisiting pan
871 evaporation trends in Australia a decade on. *Geophys. Res. Lett.* **45**, 11164–11172 (2018).

872 78 Byrne, M. P. & O’Gorman, P. A. The response of precipitation minus evapotranspiration
873 to climate warming: why the “wet-get-wetter, dry-get-drier” scaling does not hold over
874 land. *J. Clim.* **28**, 8078-8092 (2015).

875 79 Zhou, S. *et al.* Soil moisture-atmosphere feedbacks mitigate declining water availability
876 in drylands. *Nat. Clim. Change* **11**, 38–44 (2020).

877 80 Lau, W. K. & Kim, K. M. Robust Hadley Circulation changes and increasing global
878 dryness due to CO₂ warming from CMIP5 model projections. *Proc. Natl. Acad. Sci. USA*
879 **112**, 3630-3635 (2015).

880 81 Lau, W. K. M. & Tao, W. Precipitation–radiation–circulation feedback processes
881 associated with structural changes of the ITCZ in a warming climate during 1980–2014:
882 an observational portrayal. *J. Clim.* **33**, 8737-8749 (2020).

883 82 Burls, N. J. & Fedorov, A. V. Wetter subtropics in a warmer world: contrasting past and
884 future hydrological cycles. *Proc. Natl. Acad. Sci. USA* **114**, 12888-12893 (2017).

885 83 Condon, L. E., Atchley, A. L. & Maxwell, R. M. Evapotranspiration depletes
886 groundwater under warming over the contiguous United States. *Nat. Commun.* **11**, 873
887 (2020).

888 84 Jung, M. *et al.* Recent decline in the global land evapotranspiration trend due to limited
889 moisture supply. *Nature* **467**, 951-954 (2010).

890 85 García, M. *et al.* Actual evapotranspiration in drylands derived from in-situ and satellite
891 data: Assessing biophysical constraints. *Remote Sens. Environ.* **131**, 103-118 (2013).

892 86 Betts, R. A. *et al.* Projected increase in continental runoff due to plant responses to
893 increasing carbon dioxide. *Nature* **448**, 1037-1041 (2007).

894 87 Swann, A. L., Hoffman, F. M., Koven, C. D. & Randerson, J. T. Plant responses to
895 increasing CO₂ reduce estimates of climate impacts on drought severity. *Proc. Natl. Acad.*
896 *Sci. USA* **113**, 10019-10024 (2016).

897 88 Fowler, M. D., Kooperman, G. J., Randerson, J. T. & Pritchard, M. S. The effect of plant
898 physiological responses to rising CO₂ on global streamflow. *Nat. Clim. Change* **9**, 873-
899 879 (2019).

- 900 89 Lemordant, L., Gentine, P., Swann, A. S., Cook, B. I. & Scheff, J. Critical impact of
901 vegetation physiology on the continental hydrologic cycle in response to increasing CO₂.
902 *Proc. Natl. Acad. Sci. USA* **115**, 4093-4098 (2018).
- 903 90 Haverd, V. *et al.* Higher than expected CO₂ fertilization inferred from leaf to global
904 observations. *Glob. Change Biol.* **26**, 2390-2402 (2020).
- 905 91 Nie, M., Lu, M., Bell, J., Raut, S. & Pendall, E. Altered root traits due to elevated CO₂: a
906 meta-analysis. *Glob. Ecol. Biogeogr.* **22**, 1095-1105 (2013).
- 907 92 Zhang, Y. *et al.* Multi-decadal trends in global terrestrial evapotranspiration and its
908 components. *Sci. Rep.* **6**, 19124 (2016).
- 909 93 Sun, X., Wilcox, B. P. & Zou, C. B. Evapotranspiration partitioning in dryland
910 ecosystems: A global meta-analysis of in situ studies. *J. Hydrol.* **576**, 123-136 (2019).
- 911 94 Lian, X. *et al.* Partitioning global land evapotranspiration using CMIP5 models
912 constrained by observations. *Nat. Clim. Change* **8**, 640-646 (2018).
- 913 95 Yang, H., Huntingford, C., Wiltshire, A., Sitch, S. & Mercado, L. Compensatory climate
914 effects link trends in global runoff to rising atmospheric CO₂ concentration. *Environ. Res.*
915 *Lett.* **14**, 124075 (2019).
- 916 96 Mankin, J. S. *et al.* Blue water trade-offs with vegetation in a CO₂-enriched climate.
917 *Geophys. Res. Lett.* **45**, 3115-3125 (2018).
- 918 97 Stocker, B. D. *et al.* Quantifying soil moisture impacts on light use efficiency across
919 biomes. *New Phytol.* **218**, 1430-1449 (2018).
- 920 98 Liu, L. *et al.* Soil moisture dominates dryness stress on ecosystem production globally.
921 *Nat. Commun.* **11**, 4892 (2020).
- 922 99 Morgan, J. A. *et al.* C4 grasses prosper as carbon dioxide eliminates desiccation in
923 warmed semi-arid grassland. *Nature* **476**, 202-205 (2011).
- 924 100 Farrior, C. E., Rodriguez-Iturbe, I., Dybzinski, R., Levin, S. A. & Pacala, S. W. Decreased
925 water limitation under elevated CO₂ amplifies potential for forest carbon sinks. *Proc.*
926 *Natl. Acad. Sci. USA* **112**, 7213-7218 (2015).
- 927 101 Lu, X., Wang, L. & McCabe, M. F. Elevated CO₂ as a driver of global dryland greening.
928 *Sci. Rep.* **6**, 20716 (2016).
- 929 102 Ukkola, A. M., Keenan, T. F., Kelley, D. I. & Prentice, I. C. Vegetation plays an important

930 role in mediating future water resources. *Environ. Res. Lett.* **11**, 094022 (2016).

931 103 Mankin, J. S., Smerdon, J. E., Cook, B. I., Williams, A. P. & Seager, R. The curious case
932 of projected twenty-first-century drying but greening in the American west. *J. Clim.* **30**,
933 8689-8710 (2017).

934 104 Zarakas, C. M., Swann, A. L. S., Laguë, M. M., Armour, K. C. & Randerson, J. T. Plant
935 physiology increases the magnitude and spread of the transient climate response to CO₂
936 in CMIP6 Earth system models. *J. Clim.* **33**, 8561-8578 (2020).

937 105 Mankin, J. S., Seager, R., Smerdon, J. E., Cook, B. I. & Williams, A. P. Mid-latitude
938 freshwater availability reduced by projected vegetation responses to climate change. *Nat.*
939 *Geosci.* **12**, 983-988 (2019).

940 106 Song, J. *et al.* Elevated CO₂ does not stimulate carbon sink in a semi-arid grassland. *Ecol.*
941 *Lett.* **22**, 458-468 (2019).

942 107 Obermeier, W. A. *et al.* Reduced CO₂ fertilization effect in temperate C3 grasslands under
943 more extreme weather conditions. *Nat. Clim. Change* **7**, 137-141 (2016).

944 108 Craine, J. M. *et al.* Isotopic evidence for oligotrophication of terrestrial ecosystems. *Nat.*
945 *Ecol. Evol.* **2**, 1735-1744 (2018).

946 109 Medlyn, B. E. *et al.* How do leaf and ecosystem measures of water-use efficiency
947 compare? *New Phytol.* **216**, 758-770 (2017).

948 110 Keenan, T. F. *et al.* Increase in forest water-use efficiency as atmospheric carbon dioxide
949 concentrations rise. *Nature* **499**, 324-327 (2013).

950 111 Peters, W. *et al.* Increased water-use efficiency and reduced CO₂ uptake by plants during
951 droughts at a continental-scale. *Nat. Geosci.* **11**, 744-748 (2018).

952 112 Skinner, C. B., Poulsen, C. J. & Mankin, J. S. Amplification of heat extremes by plant
953 CO₂ physiological forcing. *Nat. Commun.* **9**, 1094 (2018).

954 113 Lemordant, L. & Gentine, P. Vegetation response to rising CO₂ impacts extreme
955 temperatures. *Geophys. Res. Lett.* **46**, 1383-1392 (2019).

956 114 Sellers, P. J. *et al.* Comparison of radiative and physiological effects of doubled
957 atmospheric CO₂ on climate. *Science* **271**, 1402-1406 (1996).

958 115 Warren, J. M., Norby, R. J. & Wullschleger, S. D. Elevated CO₂ enhances leaf senescence
959 during extreme drought in a temperate forest. *Tree Physiol.* **31**, 117-130 (2011).

- 960 116 De Kauwe, M. G. *et al.* Examining the evidence for decoupling between photosynthesis
961 and transpiration during heat extremes. *Biogeosciences* **16**, 903-916 (2019).
- 962 117 Huang, M. *et al.* Air temperature optima of vegetation productivity across global biomes.
963 *Nat. Ecol. Evol.* **3**, 772-779 (2019).
- 964 118 Reich, P. B., Hobbie, S. E., Lee, T. D. & Pastore, M. A. Unexpected reversal of C3 versus
965 C4 grass response to elevated CO₂ during a 20-year field experiment. *Science* **360**, 317-
966 320 (2018).
- 967 119 Norby, R. J. *et al.* Model-data synthesis for the next generation of forest free-air CO₂
968 enrichment (FACE) experiments. *New Phytol.* **209**, 17-28 (2016).
- 969 120 Steffen, W. *et al.* The emergence and evolution of Earth System Science. *Nat. Rev. Earth*
970 *Environ.* **1**, 54-63 (2020).
- 971 121 Hoekstra, A. Y. & Mekonnen, M. M. The water footprint of humanity. *Proc. Natl. Acad.*
972 *Sci. USA* **109**, 3232-3237 (2012).
- 973 122 Marvel, K. *et al.* Twentieth-century hydroclimate changes consistent with human
974 influence. *Nature* **569**, 59-65 (2019).
- 975 123 Di Baldassarre, G. *et al.* Sociohydrology: scientific challenges in addressing the
976 sustainable development goals. *Water Resour. Res.* **55**, 6327-6355 (2019).
- 977 124 van der Esch, S. *et al.* *Exploring future changes in land use and land condition and the*
978 *impacts on food, water, climate change and biodiversity: scenarios for the UNCCD*
979 *Global Land Outlook* (PBL Netherlands Environmental Assessment Agency,
980 Netherlands, 2017).
- 981 125 Gleick, P. H. Transitions to freshwater sustainability. *Proc. Natl. Acad. Sci. USA* **115**,
982 8863-8871 (2018).
- 983 126 Wada, Y., de Graaf, I. E. M. & van Beek, L. P. H. High-resolution modeling of human
984 and climate impacts on global water resources. *J. Adv. Model. Earth Syst.* **8**, 735-763
985 (2016).
- 986 127 Wada, Y. *et al.* Modeling global water use for the 21st century: the Water Futures and
987 Solutions (WFaS) initiative and its approaches. *Geosci. Model Dev.* **9**, 175-222 (2016).
- 988 **Provides an ensemble model projection of significant increases in the 21st century's**
989 **water demand by major water-use sectors under envisaged population growth and**

990 **socio-economic developments.**

991 128 Wada, Y., van Beek, L. P. H. & Bierkens, M. F. P. Nonsustainable groundwater sustaining
992 irrigation: a global assessment. *Water Resour. Res.* **48**, W00L06 (2012).

993 129 Chen, Y. *et al.* Recent global cropland water consumption constrained by observations.
994 *Water Resour. Res.* **55**, 3708-3738 (2019).

995 130 Allen, L. H., Jr., Kakani, V. G., Vu, J. C. & Boote, K. J. Elevated CO₂ increases water
996 use efficiency by sustaining photosynthesis of water-limited maize and sorghum. *J. Plant*
997 *Physiol.* **168**, 1909-1918 (2011).

998 131 Elliott, J. *et al.* Constraints and potentials of future irrigation water availability on
999 agricultural production under climate change. *Proc. Natl. Acad. Sci. USA* **111**, 3239-3244
1000 (2014).

1001 132 Urban, D. W., Sheffield, J. & Lobell, D. B. Historical effects of CO₂ and climate trends
1002 on global crop water demand. *Nat. Clim. Change* **7**, 901-905 (2017).

1003 133 Gleeson, T., Wada, Y., Bierkens, M. F. & van Beek, L. P. Water balance of global aquifers
1004 revealed by groundwater footprint. *Nature* **488**, 197-200 (2012).

1005 134 Bierkens, M. F. P. & Wada, Y. Non-renewable groundwater use and groundwater
1006 depletion: a review. *Environ. Res. Lett.* **14**, 063002 (2019).

1007 135 Rodell, M., Velicogna, I. & Famiglietti, J. S. Satellite-based estimates of groundwater
1008 depletion in India. *Nature* **460**, 999-1002 (2009).

1009 136 Feng, W. *et al.* Evaluation of groundwater depletion in North China using the Gravity
1010 Recovery and Climate Experiment (GRACE) data and ground-based measurements.
1011 *Water Resour. Res.* **49**, 2110-2118 (2013).

1012 137 Eamus, D. & Froend, R. Groundwater-dependent ecosystems: the where, what and why
1013 of GDEs. *Aust. J. Bot.* **54**, 91-96 (2006).

1014 138 Griebler, C. & Avramov, M. Groundwater ecosystem services: a review. *Freshw. Sci.* **34**,
1015 355-367 (2015).

1016 139 Devitt, T. J., Wright, A. M., Cannatella, D. C. & Hillis, D. M. Species delimitation in
1017 endangered groundwater salamanders: implications for aquifer management and
1018 biodiversity conservation. *Proc. Natl. Acad. Sci. USA* **116**, 2624-2633 (2019).

1019 140 Feng, X. *et al.* Revegetation in China's Loess Plateau is approaching sustainable water

- 1020 resource limits. *Nat. Clim. Change* **6**, 1019-1022 (2016).
- 1021 141 Hong, S. *et al.* Divergent responses of soil organic carbon to afforestation. *Nat. Sustain.*
1022 **3**, 694-700 (2020).
- 1023 142 McVicar, T. R. *et al.* Developing a decision support tool for China's re-vegetation
1024 program: Simulating regional impacts of afforestation on average annual streamflow in
1025 the Loess Plateau. *Forest Ecol. Manag.* **251**, 65-81 (2007).
- 1026 143 Zhao, M. *et al.* Ecological restoration impact on total terrestrial water storage. *Nat.*
1027 *Sustain.* **4**, 56–62 (2020).
- 1028 144 Kwon, H.-Y. *et al.* in *Economics of Land Degradation and Improvement – A Global*
1029 *Assessment for Sustainable Development* (eds Nkonya E., Mirzabaev A., von Braun J.)
1030 Ch. 8, 197-214 (Springer International Publishing, 2016).
- 1031 145 Asner, G. P., Elmore, A. J., Olander, L. P., Martin, R. E. & Harris, A. T. Grazing systems,
1032 ecosystem responses, and global change. *Annu. Rev. Environ. Resour.* **29**, 261-299
1033 (2004).
- 1034 146 Dunne, T., Western, D. & Dietrich, W. E. Effects of cattle trampling on vegetation,
1035 infiltration, and erosion in a tropical rangeland. *J. Arid Environ.* **75**, 58-69 (2011).
- 1036 147 Griscom, B. W. *et al.* Natural climate solutions. *Proc. Natl. Acad. Sci. USA* **114**, 11645-
1037 11650 (2017).
- 1038 148 Lewis, S. L., Wheeler, C. E., Mitchard, E. T. & Koch, A. Restoring natural forests is the
1039 best way to remove atmospheric carbon. *Nature* **568**, 25-28 (2019).
- 1040 149 Reisman-Berman, O., Keasar, T. & Tel-Zur, N. Native and non-native species for dryland
1041 afforestation: bridging ecosystem integrity and livelihood support. *Ann. For. Sci.* **76**, 114
1042 (2019).
- 1043 150 Zhang, J. *et al.* Carrying capacity for vegetation across northern China drylands. *Sci. Total*
1044 *Environ.* **710**, 136391 (2020).
- 1045 151 Liu, Y., Kumar, M., Katul, G. G. & Porporato, A. Reduced resilience as an early warning
1046 signal of forest mortality. *Nat. Clim. Change* **9**, 880-885 (2019).
- 1047 152 Fita, A., Rodríguez-Burruezo, A., Boscaiu, M., Prohens, J. & Vicente, O. Breeding and
1048 domesticating crops adapted to drought and salinity: a new paradigm for increasing food
1049 production. *Front. Plant Sci.* **6**, 978 (2015).

1050 153 Graham, N. T. *et al.* Water sector assumptions for the Shared Socioeconomic Pathways
1051 in an integrated modeling framework. *Water Resour. Res.* **54**, 6423-6440 (2018).

1052 154 Muhs, D. R. The geologic records of dust in the Quaternary. *Aeolian Res.* **9**, 3-48 (2013).

1053 155 Scheff, J., Seager, R., Liu, H. & Coats, S. Are glacials dry? consequences for
1054 paleoclimatology and for greenhouse warming. *J. Clim.* **30**, 6593-6609 (2017).

1055 156 Lambert, F. *et al.* Dust-climate couplings over the past 800,000 years from the EPICA
1056 Dome C ice core. *Nature* **452**, 616-619 (2008).

1057 157 Salzmann, U. *et al.* Climate and environment of a Pliocene warm world. *Palaeogeogr.*
1058 *Palaeoclimatol. Palaeoecol.* **309**, 1-8 (2011).

1059 158 Fu, Q., Lin, L., Huang, J., Feng, S. & Gettelman, A. Changes in terrestrial aridity for the
1060 period 850–2080 from the Community Earth System Model. *J. Geophys. Res. Atmos.* **121**,
1061 2857-2873 (2016).

1062 159 Prudhomme, C. *et al.* Hydrological droughts in the 21st century, hotspots and
1063 uncertainties from a global multimodel ensemble experiment. *Proc. Natl. Acad. Sci. USA*
1064 **111**, 3262-3267 (2014).

1065 160 Cook, B. I., Ault, T. R. & Smerdon, J. E. Unprecedented 21st century drought risk in the
1066 American Southwest and Central Plains. *Sci. Adv.* **1**, e1400082 (2015).

1067 161 Ault, T. R. On the essentials of drought in a changing climate. *Science* **368**, 256-260
1068 (2020).

1069 162 Reichstein, M. *et al.* Climate extremes and the carbon cycle. *Nature* **500**, 287-295 (2013).

1070 163 Anderegg, W. R. L., Kane, J. M. & Anderegg, L. D. L. Consequences of widespread tree
1071 mortality triggered by drought and temperature stress. *Nat. Clim. Change* **3**, 30-36 (2012).

1072 164 Williams, A. P. *et al.* Forest responses to increasing aridity and warmth in the
1073 southwestern United States. *Proc. Natl. Acad. Sci. USA* **107**, 21289-21294 (2010).

1074 165 Pellegrini, A. F. A. *et al.* Fire frequency drives decadal changes in soil carbon and
1075 nitrogen and ecosystem productivity. *Nature* **553**, 194-198 (2018).

1076 166 Bowman, D. M. J. S. *et al.* Vegetation fires in the Anthropocene. *Nat. Rev. Earth Environ.*
1077 **1**, 500–515 (2020).

1078 167 Andela, N. *et al.* A human-driven decline in global burned area. *Science* **356**, 1356-1362
1079 (2017).

- 1080 168 Pechony, O. & Shindell, D. T. Driving forces of global wildfires over the past millennium
1081 and the forthcoming century. *Proc. Natl. Acad. Sci. USA* **107**, 19167-19170 (2010).
- 1082 169 Hoover, D. L., Knapp, A. K. & Smith, M. D. Resistance and resilience of a grassland
1083 ecosystem to climate extremes. *Ecology* **95**, 2646-2656 (2014).
- 1084 170 Greve, P. *et al.* Global assessment of water challenges under uncertainty in water scarcity
1085 projections. *Nat. Sustain.* **1**, 486-494 (2018).
- 1086 171 Scanlon, B. R. *et al.* Global models underestimate large decadal declining and rising water
1087 storage trends relative to GRACE satellite data. *Proc. Natl. Acad. Sci. USA* **115**, E1080-
1088 E1089 (2018).
- 1089 172 Abatzoglou, J. T., Dobrowski, S. Z., Parks, S. A. & Hegewisch, K. C. TerraClimate, a
1090 high-resolution global dataset of monthly climate and climatic water balance from 1958-
1091 2015. *Sci. Data* **5**, 170191 (2018).
- 1092 173 Roderick, M. L., Sun, F., Lim, W. H. & Farquhar, G. D. A general framework for
1093 understanding the response of the water cycle to global warming over land and ocean.
1094 *Hydrol. Earth Syst. Sci.* **18**, 1575-1589 (2014).
- 1095 174 Gudmundsson, L., Greve, P. & Seneviratne, S. I. The sensitivity of water availability to
1096 changes in the aridity index and other factors—a probabilistic analysis in the Budyko
1097 space. *Geophys. Res. Lett.* **43**, 6985-6994 (2016).
- 1098 175 American Meteorological Society. *Glossary of Meteorology*. [http://](http://http://glossary.ametsoc.org/wiki/Aridity)
1099 <http://glossary.ametsoc.org/wiki/Aridity> (2000).
- 1100 176 Allen, R. G., Pereira, L. S., Raes, D. & Smith, M. Crop Evapotranspiration — Guidelines
1101 for Computing Crop Water Requirements FAO Irrigation and Drainage Paper No. 56
1102 (FAO, 1998).
- 1103 177 Dai, A. Drought under global warming: a review. *Wiley Interdiscip. Rev. Clim. Chang.* **2**,
1104 45-65 (2011).
- 1105 178 Dai A. Historical and future changes in streamflow and continental runoff: a review. In:
1106 *Terrestrial water cycle and climate change: natural and human-induced impacts*,
1107 *Geophys. Monogr.* (eds. Tang Q. and Oki T.) 1st edn, Ch. 2, 17-37 (Wiley, 2016).
- 1108 179 Sitch, S. *et al.* Trends and drivers of regional sources and sinks of carbon dioxide over
1109 the past two decades. *Biogeosciences Discuss.* **10**, 20113-20177 (2013).

- 1110 180 Donohue, R. J., Roderick, M. L., McVicar, T. R. & Yang, Y. A simple hypothesis of how
1111 leaf and canopy-level transpiration and assimilation respond to elevated CO₂ reveals
1112 distinct response patterns between disturbed and undisturbed vegetation. *J. Geophys. Res.*
1113 *Biogeosciences* **122**, 168-184 (2017).
- 1114 181 Barton, C. V. M. *et al.* Effects of elevated atmospheric [CO₂] on instantaneous
1115 transpiration efficiency at leaf and canopy scales in *Eucalyptus saligna*. *Glob. Change*
1116 *Biol.* **18**, 585-595 (2012).
- 1117 182 Savvides, A. M. & Fotopoulos, V. Two inexpensive and non-destructive techniques to
1118 correct for Smaller-Than-Gasket Leaf Area in gas exchange measurements. *Front. Plant*
1119 *Sci.* **9**, 548-548 (2018).

1120 **Acknowledgements**

1121 This study was supported by National Natural Science Foundation of China (41991230, 41988101),
1122 the Second Tibetan Plateau Scientific Expedition and Research Program (Grant
1123 No.2019QZKK0405) and the Xplorer Prize.

1124

1125 **Author contributions**

1126 S.P., formulated the review and identified the themes to be covered. X.L. performed the analyses
1127 and drafted the figures. X.L., S.P. and A.C. wrote the first draft of the manuscript. C.H., B.F.,
1128 L.Z.X.L., J.H., J.S., A.M.B., T.F.K., T.R.M., Y.W., X.W., T.W., Y.Y., M.L.R. reviewed and edited
1129 the manuscript before submission. All authors made substantial contributions to the discussion of
1130 content.

1131

1132 **Competing interests**

1133 The authors declare no competing interests.

1134

1135 **Peer review information**

1136 Nature Reviews Earth & Environment thanks Aristeidis Koutroulis, Sujong Jeong and the other,
1137 anonymous, reviewer(s) for their contribution to the peer review of this work.

1138

1139 **Publisher's note**

1140 Springer Nature remains neutral with regard to jurisdictional claims in published maps and
1141 institutional affiliations.

1142

1143 **Supplementary information**

1144 Supplementary information is available for this paper at <https://doi.org/10.1038/s415XX-XXX->

1145 XXXX-X

1146

1147 **Key points**

- 1148 1. Atmospheric, agricultural, hydrological and ecological indices of aridity reveal strongly
1149 divergent trends since 1950 and into the near future.
- 1150 2. Warming-driven increases in vapour pressure deficit hastens evaporative water loss and
1151 depletes surface moisture, in turn, amplifying atmospheric drying through land-atmosphere
1152 feedbacks.
- 1153 3. Plant stomatal closure under elevated CO₂ reduces transpiration and compensates for the
1154 adverse effect of higher vapour pressure deficit for plant growth, explaining the co-occurrence
1155 of ecosystem greening and atmospheric drying in drylands.
- 1156 4. The physiologically-induced lowering of evapotranspiration under rising CO₂, along with the
1157 strong limitation by soil moisture, disconnects atmospheric drying and hydrological responses
1158 in drylands.
- 1159 5. With rapid climate change and population growth, anthropogenic water demand in drylands is
1160 projected to increase by ~270% by 2090s, exacerbating current water-resource scarcity.
- 1161 6. As future water deficits are driven mainly by increasing water demand, sustainable water-
1162 resource management and water-conservation technologies are needed to balance the socio-
1163 economic demands for water resources while maintaining healthy dryland ecosystems.

1164

1165

1166

1167

1168

1169

1170

Table 1. Trend statistics for different aridity metrics and databases.

Metric database	and	Averaged change over the global dryland			Areal change of the global dryland (% decade ⁻¹)		
		1948-2016	1979-2016	Near future	1948-2016	1979-2016	Near future
Data-based VPD (10 ⁻² kPa yr ⁻¹)		0.12 ± 0.01 (**)	0.16 ± 0.02 (**)	—	0.55 ± 0.11 (**)	1.49 ± 0.19 (**)	—
ESMs VPD (10 ⁻² kPa yr ⁻¹)		0.15 ± 0.002 (1948-2005, **)	0.25 ± 0.04 (1979-2005, **)	0.21 ± 0.01 (2006-2100, **)	0.65 ± 0.07 (1948-2005, **)	1.15 ± 0.21 (1979-2005, **)	1.01 ± 0.03 (2006-2100, **)
Data-based AI (10 ⁻³ yr ⁻¹)		-0.02 ± 0.08 (n.s.)	-0.13 ± 0.12 (n.s.)	—	0.13 ± 0.06 (**)	0.05 ± 0.15 (n.s.)	—
Data-based AI_CO ₂ (10 ⁻³ yr ⁻¹)		0.04 ± 0.08 (n.s.)	0.20 ± 0.12 (n.s.)	—	0.08 ± 0.06 (n.s.)	-0.02 ± 0.15 (n.s.)	—
ESMs AI (10 ⁻³ yr ⁻¹)		-0.07 ± 0.04 (1948-2005, *)	0.16 ± 0.15 (1979-2005, n.s.)	-0.11 ± 0.02 (2006-2100, **)	0.14 ± 0.03 (1948-2005, **)	0.02 ± 0.10 (1979-2005, *)	0.20 ± 0.02 (2006-2100, **)
ESMs AI_CO ₂ (10 ⁻³ yr ⁻¹)		-0.03 ± 0.04 (1948-2005, n.s.)	0.20 ± 0.15 (1979-2005, n.s.)	-0.07 ± 0.02 (2006-2100, **)	0.11 ± 0.03 (1948-2005, **)	-0.03 ± 0.10 (1979-2005, n.s.)	0.15 ± 0.01 (2006-2100, **)
GLDAS soil moisture (% yr ⁻¹)		-0.015 ± 0.007 (1948-2010, **)	0.014 ± 0.016 (1979-2010, n.s.)	—	0.09 ± 0.08 (1948-2010, n.s.)	-0.12 ± 0.18 (1979-2010, n.s.)	—
TerraClimate soil moisture (% yr ⁻¹)		-0.061 ± 0.038 (1980-2016, n.s.)	0.032 ± 0.052 (1980-2016, n.s.)	—	0.05 ± 0.05 (1958-2015, n.s.)	-0.12 ± 0.10 (1979-2015, n.s.)	—
GLEAM soil moisture (% yr ⁻¹)		—	0.047 ± 0.022 (1980-2016, **)	—	—	-0.22 ± 0.16 (1980-2016, n.s.)	—
DGVMs soil moisture (% yr ⁻¹)		-0.017 ± 0.009 (**)	-0.045 ± 0.017 (n.s.)	—	0.09 ± 0.05 (*)	0.13 ± 0.10 (n.s.)	—
ESMs soil moisture (% yr ⁻¹)		-0.010 ± 0.002 (1948-2005, **)	-0.026 ± 0.006 (1979-2005, **)	-0.014 ± 0.001 (2006-2100, **)	0.05 ± 0.02 (1948-2005, **)	0.06 ± 0.05 (1979-2005, n.s.)	0.13 ± 0.01 (2006-2100, **)
River records (mm yr ⁻²)		-0.192 ± 0.120 (1948-2016, n.s.)	0.203 ± 0.190 (1948-2016, n.s.)	—	—	—	—
LORA runoff (mm yr ⁻²)		—	0.106 ± 0.055 (1980-2012, *)	—	—	-0.33 ± 0.16 (1980-2012, **)	—
DGVMs runoff (mm yr ⁻²)		-0.075 ± 0.038 (**)	0.012 ± 0.076 (n.s.)	—	0.06 ± 0.07 (n.s.)	-0.21 ± 0.16 (n.s.)	—
ESMs runoff (mm yr ⁻²)		-0.005 ± 0.010 (1948-2005, n.s.)	0.021 ± 0.036 (1979-2005, n.s.)	0.011 ± 0.005 (2006-2100, **)	0.03 ± 0.02 (1948-2005, *)	-0.17 ± 0.08 (1979-2005, **)	-0.02 ± 0.01 (2006-2100, *)
GIMMS NDVI (10 ⁻² yr ⁻¹)		—	0.024 ± 0.006 (1982-2016, **)	—	—	-0.64 ± 0.14 (1982-2016, **)	—
MODIS LAI (10 ⁻² yr ⁻¹)		—	0.33 ± 0.06 (2000-2016, **)	—	—	-1.55 ± 0.19 (2000-2016, **)	—
DGVMs GPP (gC m ⁻² yr ⁻²)		1.0 ± 0.1 (**)	1.4 ± 0.2 (**)	—	-0.72 ± 0.04 (**)	-0.95 ± 0.10 (**)	—
ESMs GPP (gC m ⁻² yr ⁻²)		1.5 ± 0.0 (1948-2005, **)	1.6 ± 0.1 (1979-2005, **)	1.4 ± 0.0 (2006-2100, **)	-0.75 ± 0.02 (1948-2005, **)	-0.95 ± 0.06 (1979-2005, **)	-0.67 ± 0.02 (2006-2100, **)

1172 Slope (± 1-S.D.) and statistical significance of the linear regression against time for each aridity metric and database. Unless
1173 otherwise stated in parentheses, the period over which trends are quantified are shown in the column heading. Statistical significance
1174 is determined using a *t*-test, with symbols “***”, “**” and “n.s.” denoting $p < 0.05$, $p < 0.1$ and $p > 0.1$, respectively. Trends for vapour
1175 pressure deficit (VPD) and aridity index (AI) are calculated using the mean of multiple datasets, and those for Dynamic Global
1176 Vegetation Models (DGVMs) and CMIP5 Earth System Models (ESMs) using the mean of multiple models. Note that the trend
1177 unit for averaged change is metric-dependent, but that for areal change it is the same across metrics (% decade⁻¹).

1179 **Figure 1 | Global drylands and ecohydrological conditions.** The extent and classification of
1180 Aridity Index-defined drylands for 1961-1990, based on the TerraClimate dataset with high (~4
1181 km) spatial resolution¹⁷². The cyan dots illustrate the density of vegetation cover for 1982-1990
1182 (based on the GIMMS Normalized Difference Vegetation Index), with larger dots indicating denser
1183 vegetation cover. Note that all analyses in Figs. 2 and 3 focus solely on warm drylands (drylands
1184 south of 50°N), where all land surface elements routinely experience water stress.

1185
1186 **Figure 2 | Past and future dryland changes evaluated by five different aridity metrics. a-e |**
1187 Various observational and model-derived anomalies of vapour pressure deficit (VPD) (**panel a**),
1188 aridity index (AI) or AI_CO₂ that additionally accounts for CO₂ physiological impacts (**panel b**),
1189 soil moisture (**panel c**), runoff (**panel d**) and gross primary production (GPP), normalized
1190 difference vegetation index (NDVI) and leaf area index (LAI) (**panel e**), all averaged over AI-
1191 defined baseline regions of drylands for 1961-1990. **f-j |** as in a-e, but anomalies of the fraction of
1192 water-stressed land areas (drylands) evaluated by VPD (f_{atm}) (**panel f**), AI (f_{AI} or $f_{\text{AI_CO}_2}$) (**panel g**),
1193 soil moisture (f_{soil}) (**panel h**), runoff (f_{hyd}) (**panel i**) and GPP, NDVI or LAI (f_{veg}) (**panel j**). Similar
1194 to f_{AI} (regions with AI < 0.65), f_{atm} , f_{soil} , f_{hyd} and f_{veg} are computed using threshold values of the
1195 corresponding metric (**Supplementary Methods**). Anomalies are computed by subtracting the
1196 climatological mean of 1961-1990 (or a subset of years during this period depending on the
1197 temporal coverage of data). The shaded areas represent the 95% confidence intervals of multiple
1198 data sources (for VPD and AI) or model results (for Dynamic Global Vegetation Models (DGVMs)
1199 or Earth System Models (ESMs)). The ESM results are derived from CMIP5 under the “historical”
1200 (1948-2005) and “RCP4.5” (2006-2100) scenarios. These different metrics present divergence in
1201 aridity changes and rates of global dryland expansion in both the past and the future. Trends of
1202 each metric and dataset are summarized in **Table 1**.

1203
1204 **Figure 3 | Continental assessment of future dryland changes.** Projected future changes in the
1205 fraction of drylands and the four dryland subcategories (dry sub-humid, semi-arid, arid and hyper-
1206 arid; columns) as presented by f_{atm} (**panels a-e**), f_{AI} and $f_{\text{AI_CO}_2}$ (**panels f-j**, left and right half of
1207 symbols, respectively), f_{soil} (**panels k-o**), f_{hyd} (**panels p-t**) and f_{veg} (**panels u-y**). Each circle
1208 represents the difference between dryland area (as a percentage of the sub-continent area) of a
1209 future period (1.5°C or 2°C warmer than the pre-industrial level, or the 2090s; all under the CMIP5
1210 RCP4.5 scenario) and that of the 1961-1990 baseline (under the CMIP5 historical scenario).

1211 Changes in f_{atm} , f_{soil} , f_{hyd} and f_{veg} are computed using threshold values of the corresponding metric
1212 (Supplementary Methods). Continental dryland regions labelled “I-VI” are marked with red boxes
1213 in panel **z**, which also illustrates the spatial distribution of regions where vegetation growth
1214 indicates a conversion from drylands to non-drylands in the near future (for 1.5 °C warmer, 2 °C
1215 warmer or the 2090s, relative to 1961-1990), corresponding to panels **u-y**. It is projected that in the
1216 future, the global dryland area will expand based on f_{atm} , f_{AI} and f_{soil} , but contract based on f_{hyd} and
1217 f_{veg} , with regionally dependent magnitude and/or sign of changes.

1218
1219 **Figure 4 | Physical and physiological mechanisms for dryland aridity changes. a** | Schematic
1220 representation of processes underlying aridity changes of the atmospheric, hydrological, ecological
1221 and socio-economic systems, under warming and rising atmospheric CO₂. Circled symbols of ‘-’,
1222 ‘+’ and ‘?’ represent a negative, positive or potentially unknown sign of impact, respectively. **b** |
1223 Mechanisms for the shifting partitioning of precipitation between AET and runoff under warming
1224 and elevated CO₂. The curve shows the Budyko framework^{173,174} that links the partitioning of
1225 precipitation (P) into AET (green shaded area) and runoff (blue shaded area) to surface aridity level
1226 (defined by AI). The symbol ‘Δ’ denotes change of the corresponding quantity under warming and
1227 elevated CO₂. Under conditions of warming and decreasing AI values, the AET increase (vertical
1228 black arrow) cannot keep up with the PET increase (horizontal black arrow), owing to the water
1229 limitations and the physiological regulations of plant water loss under elevated CO₂.

1230
1231 **Figure 5 | Dryland anthropogenic water stress under climatic and socio-economic changes.**
1232 Historical and future changes of total anthropogenic water for North America (**panel a**), Northern
1233 Africa (**panel b**), Eurasia (**panel c**), South America (**panel d**), Southern Africa (**panel d**), Australia
1234 (**panel e**), and global drylands (**panel g**); for map of regions, see Fig. 3z. The water demand (D) is
1235 presented as a sum of agricultural, domestic and industrial water withdrawal, and the water supply
1236 (S) is mainly surface runoff. The y-axis scale is different for D and S. The time series are derived
1237 from the ensemble mean of three global hydrological models (GHMs, including H08, MATSIRO
1238 and LPJml) under the SSP2-RCP6.0 scenario. Arrows show the amount of D and S during 2090s,
1239 with numbers on the right showing the relative changes to the 1961-1990 baseline.

1240

1241 **Figure 6 | Conceptual diagram of future dryland aridity changes.** Present-day (**panel a**) versus
1242 future (**panel b**) aridity conditions of the atmospheric, hydrological, ecological and socio-economic
1243 systems over drylands. Future changes of dryland ecohydrological variables are based on CMIP5
1244 simulations, without accounting for direct human interference. In panel **b**, red symbols of ‘+’ and
1245 ‘-’ in brackets represent an overall increase and decrease in the corresponding quantity respectively,
1246 relative to its present-day level. Note that the potential spatial heterogeneity of ecohydrological
1247 changes is not illustrated. The anticipated water demand changes (in dashed arrow) of the human
1248 society are based on global hydrological model simulations. VPD: vapour pressure deficit.

1249
1250
1251
1252
1253
1254
1255
1256
1257
1258
1259
1260
1261
1262
1263
1264
1265
1266
1267
1268
1269

1270 **Box 1. The multifaceted features and definitions of “aridity”.**

1271 Aridity is a long-term state of water scarcity, which measures “the degree to which a climate lacks
1272 effective, life-promoting moisture”¹⁷⁵. In this sense, aridity is essentially different from drought
1273 which tracks short-term (days to years) departures from normal surface water conditions. Owing
1274 to the limited availability of surface soil moisture measurements, the Aridity Index (AI) which only
1275 requires meteorological measurements is popular in dryland studies. AI calculates the balance
1276 between the atmospheric water supply to the land (precipitation) and its demand from the land
1277 surface (potential evapotranspiration, PET). The PET formulation is often based on the Penman-
1278 Monteith equation¹⁷⁶ that requires meteorological inputs of net solar radiation (R_n), temperature
1279 (T), vapour pressure deficit (D), 2-m wind speed (u_2), psychrometric constant (γ), and the slope
1280 of saturation vapour-pressure with temperature (Δ) (Eqn. 1).

$$\text{PET} = \frac{0.408\Delta R_n + \gamma \frac{900}{T + 273} u_2 D}{\Delta + \gamma \left(1 + (0.34 + 0.00024(c_a - 300))u_2\right)} \quad (1)$$

1281 Where $0.00024(c_a - 300)$ accounts for the effect of rising atmospheric CO₂ concentration (c_a , ppm)
1282 on surface stomatal resistance (fixed as 0.34 in the original PET parameterisation), with the
1283 coefficients estimated from CMIP5 model outputs forced by rising c_a under non-water-stressed
1284 conditions⁴⁵. Drylands are traditionally defined by the United Nations Environment Programme⁴²
1285 as areas with $\text{AI} \leq 0.65$, and can be further sub-categorised into dry sub-humid ($0.65 > \text{AI} \geq 0.5$),
1286 semi-arid ($0.5 > \text{AI} \geq 0.2$), arid ($0.2 > \text{AI} \geq 0.05$) and hyper-arid ($\text{AI} < 0.05$) regions^{10,42}.

1287
1288 Importantly, aridity itself is a highly complex concept on which there are numerous specific
1289 perspectives. Atmospheric aridity describes high atmospheric demand for water, and is measured
1290 by VPD or relative humidity^{48,72}; soil moisture (or agricultural) aridity describes a state of soil

1291 moisture stress^{57,177}; hydrological aridity describes a deficit of surface runoff¹⁷⁸; ecological aridity
1292 describes a state of insufficient moisture to support vegetation growth, and is often related to
1293 reduction (or reduced capacity) of plant photosynthetic uptake of CO₂ (ref. ³⁶).

1294
1295 Although aridity means an excess of water demand over available supply for all Earth system
1296 processes, both the demand and supply sides differ substantially among them^{36,37,40,46,155}. For
1297 instance, soil moisture is supplied by precipitation and glacier melt water, and the water demand is
1298 determined by plant transpiration and soil evaporation. Plants extract moisture from soils to live
1299 and grow, and the water demand is determined by atmospheric dryness and plant physiology³⁷.
1300 Livestock and humans demand water to survive, which is provided mostly by rivers, lakes and
1301 groundwater reservoirs. Such different Earth system processes involved in the depiction of demand
1302 and supply for water cause these metrics to diverge in response to elevated CO₂.

1303

1304 **Box 2. Characterising CO₂ physiological impacts on dryland productivity**

1305 Owing to the confounding effect of climate change, it is difficult to quantify dryland ecosystem
1306 responses to elevated CO₂ with empirical statistical models and historical records. Dynamic Global
1307 Vegetation Models (DGVMs) (**Supplementary Table 2**) participating in the “Trends in net land-
1308 atmosphere carbon exchange” (TRENDY; **Supplementary Methods**) project enable the
1309 quantitative characterisation of CO₂ physiological forcings, for example, using the simulation S1
1310 forced by varying CO₂ but fixed climate¹⁷⁹. Higher CO₂ enhances gross primary production (GPP)
1311 through two parallel physiological processes: the direct CO₂ fertilization effect that enhances
1312 productivity while simultaneously consumes more water; and the indirect physiological effect
1313 which reduces stomatal conductance and thus conserves water for additional carbon uptake. The
1314 following analysis extracts contributions of the two counteracting mechanisms to dryland GPP
1315 changes.

1316

1317 GPP can be represented as the product of canopy-scale transpiration (E_t) and canopy-scale water-
1318 use efficiency (WUE_c):

$$GPP = E_t \cdot WUE_c \quad (2)$$

1319 By applying a differential transformation, fractional GPP changes are presented as:

$$\frac{dGPP}{GPP_0} = \frac{dE_t}{E_{t0}} + \frac{dWUE_c}{WUE_{c0}} \quad (3)$$

1320 where the subscript ‘0’ denotes the value for a baseline period (1948-1957). For a fixed
1321 precipitation amount, the strong water limitation for dryland ecosystems determines that E_t is
1322 approximately conserved²⁸. For example, DGVMs (in the simulation forced by both varying CO₂

1323 and climate) estimate a slight E_t increase by +0.9% from 1948-1957 to 2007-2016. Hence, WUE_c
 1324 changes can almost fully explain the CO_2 -driven increase of dryland GPP.

1325
 1326 Warm and arid ecosystems often have simple aboveground structure, typically with leaf area index
 1327 (L) less than unity. This means that an increase in L would usually capture, linearly, more light and
 1328 thus be proportionally related to enhanced transpiration and productivity^{28,180}. Hence, leaf-level
 1329 CO_2 assimilation (A) and water loss ($E_{t,l}$) can be approximated as GPP and transpiration per unit
 1330 leaf area (Eqn. 4). Under this assumption, WUE_c can be directly scaled from the WUE of individual
 1331 leaves (WUE_l) (Eqn. 5), as robustly supported by field experiments^{181,182}. Hence,

$$E_t = \int E_{t,l} \approx E_{t,l}L; \quad GPP = \int A \approx AL \quad (4)$$

$$WUE_c \approx WUE_l = \frac{A}{E_{t,l}} \quad (5)$$

1332 By integrating Eqns. 3-5 to Eqn. 6, fractional changes of WUE_c can be separated into contributions
 1333 from changes of leaf-level carbon and water fluxes.

$$\frac{dWUE_c}{WUE_{c0}} \approx \frac{dWUE_l}{WUE_{l0}} = \frac{dA}{A} + \left(-\frac{dE_{t,l}}{E_{t,l0}} \right) \quad (6)$$

1334 Eqn. 6 enables a disaggregation of the two physiological response. The first term (dA/A_0) can be
 1335 interpreted as the leaf-scale CO_2 fertilization effect, and the second term ($-dE_{t,l}/E_{t,l0}$) as the leaf-
 1336 scale CO_2 water savings effect. By integrating these equations and DGVM simulations, the water-
 1337 saving effect is estimated to contribute 52% of the dryland GPP increase from 1948-1957 to 2007-
 1338 2016, much higher than the effect of CO_2 fertilization (18%) and climate change (18%).

1339

1340

1341 **Toc Blurb**

1342 Estimates of global dryland changes are often conflicting. This Review discusses and quantifies observed
1343 and projected aridity changes, revealing divergent responses between atmospheric and ecohydrological
1344 metrics that can be explained by plant physiological responses to elevated CO₂.

1345

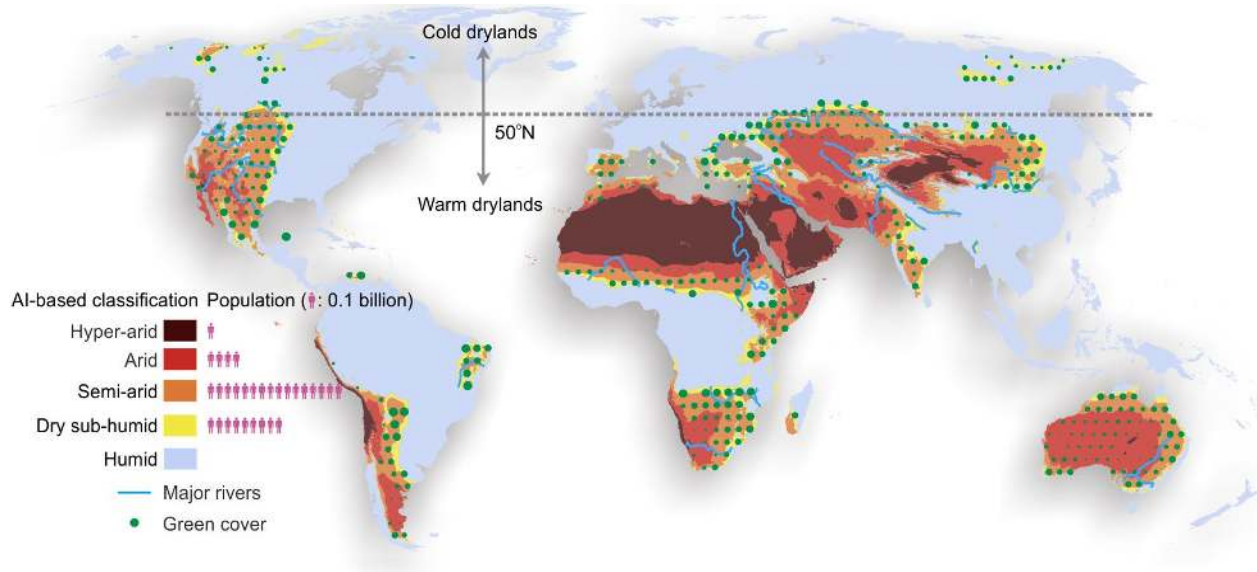
1346

1347

1348

1349

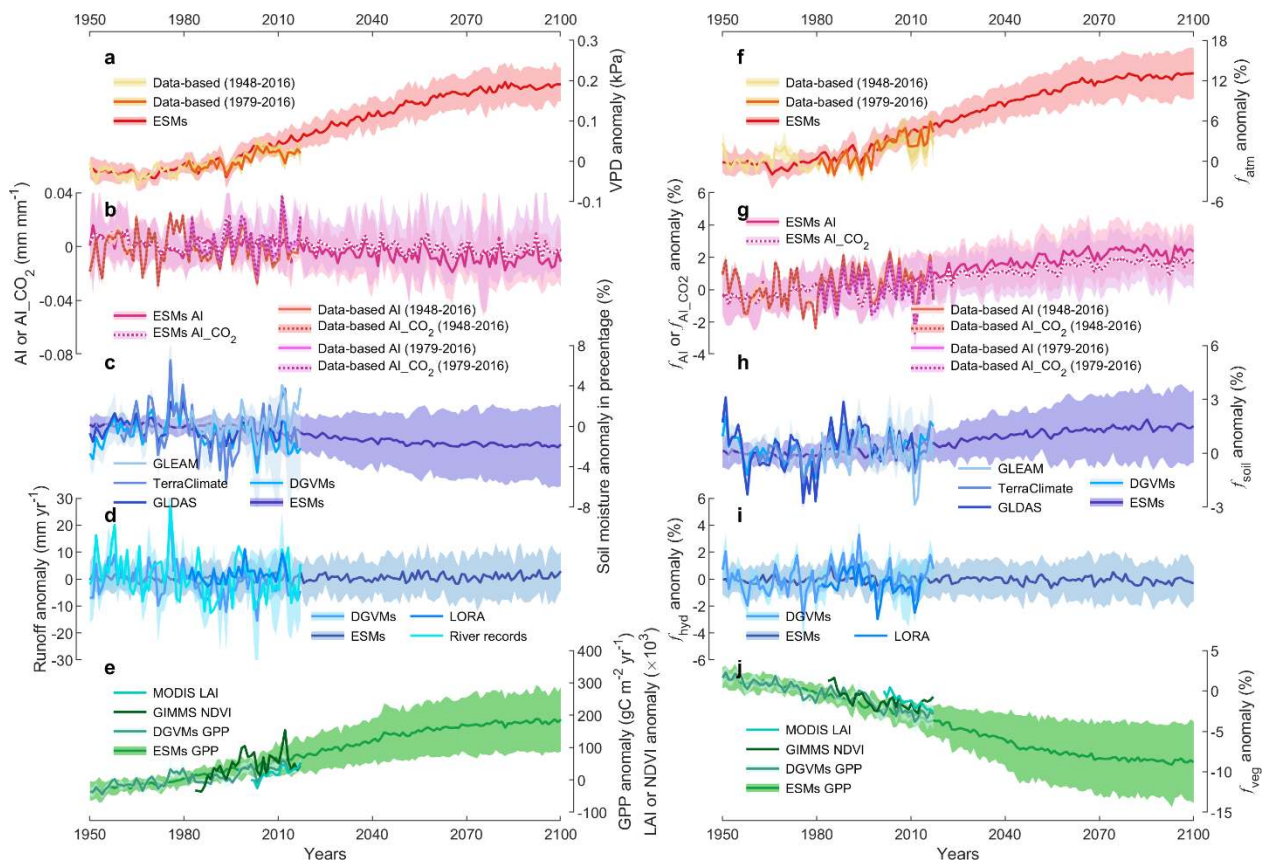
1350 **Figure 1 | Global drylands and ecohydrological conditions.** The global map shows the extent
1351 and classification of AI-defined drylands for 1961-1990, based on the TerraClimate dataset with
1352 high (~4 km) spatial resolution¹⁶⁹. The cyan dots show the density of vegetation cover for 1982-
1353 1990 (based on the GIMMS NDVI), with larger dots indicating denser vegetation cover. Note
1354 that all analyses in Figs. 2 and 3 focus solely on warm drylands (drylands south of 50°N), where
1355 all land surface elements routinely experience water stress.



1356

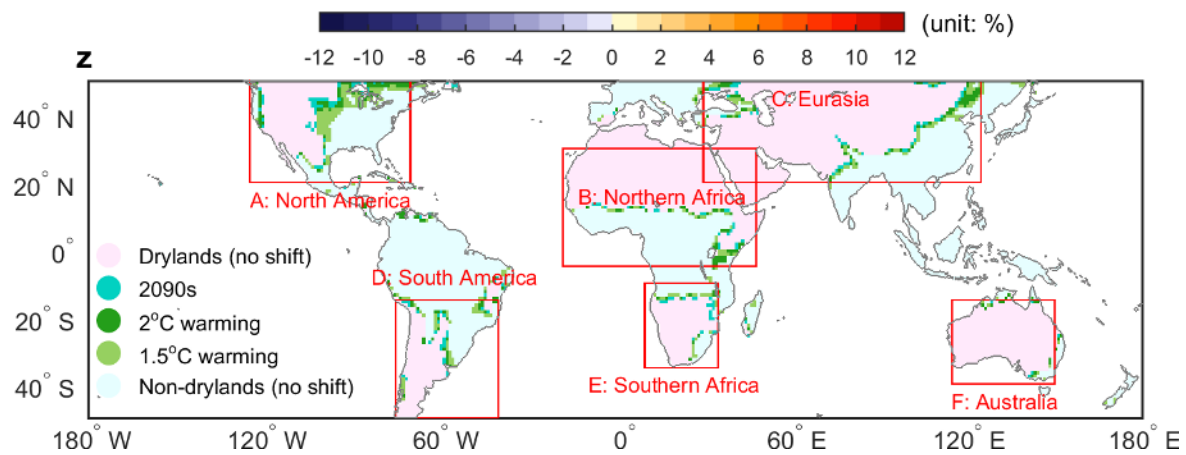
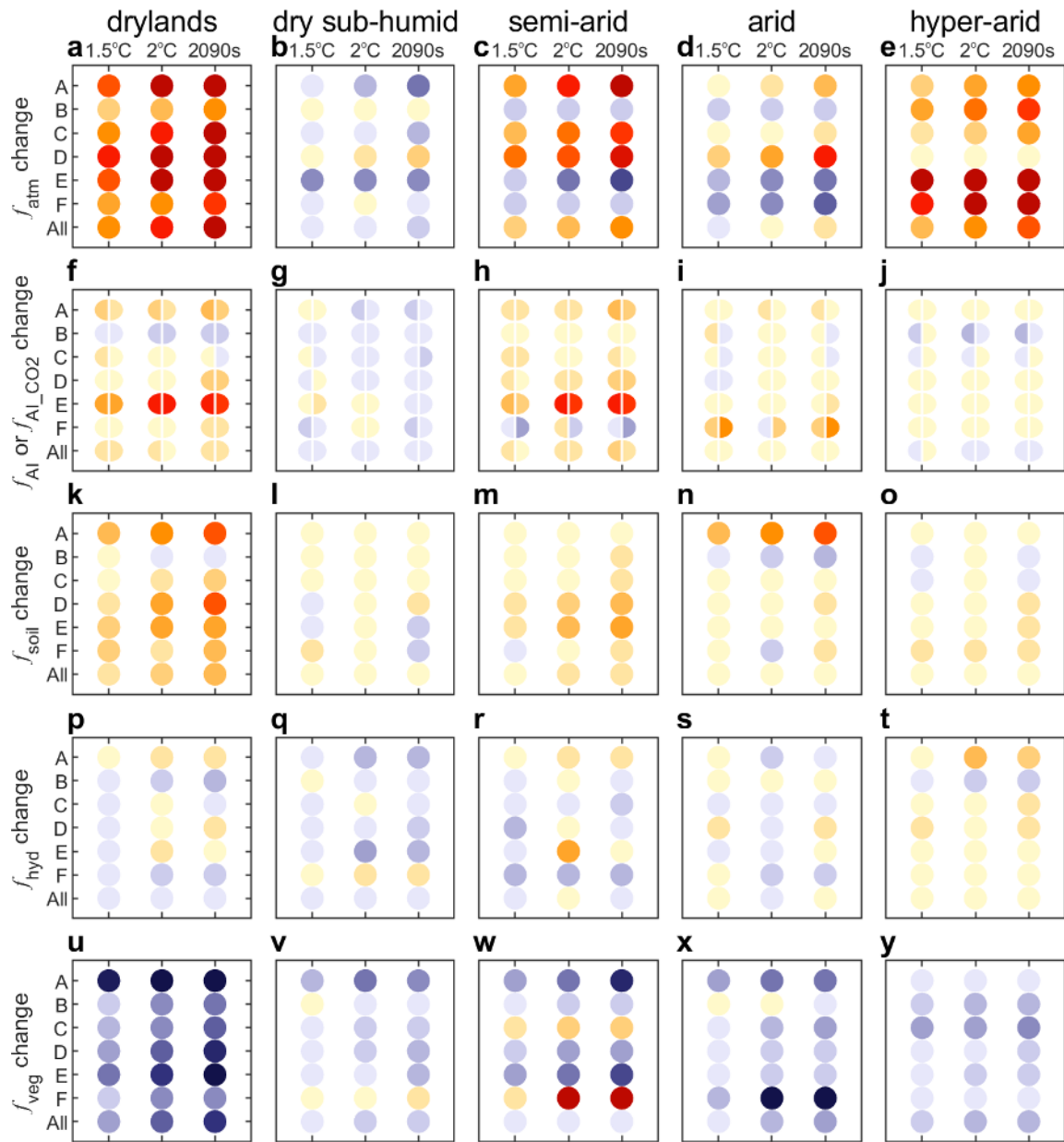
1357

1358 **Figure 2 | Past and future dryland changes evaluated by five different aridity metrics. a-e |**
 1359 **Anomalies of VPD (a), AI (or AI_CO2 that additionally accounts for CO2 physiological impacts)**
 1360 **(b), soil moisture (c), runoff (d) and GPP, NDVI or LAI (e), averaged over AI-defined baseline**
 1361 **regions of drylands for 1961-1990. f-j | Anomalies of the fraction of water-stressed land areas**
 1362 **(drylands) evaluated by VPD (f_{atm}) (f), AI (f_{AI} or $f_{AI_CO_2}$) (g), soil moisture (f_{soil}) (h), runoff (f_{hyd}) (i)**
 1363 **and GPP, NDVI or LAI (f_{veg}) (j). Similar to f_{AI} (regions with $AI < 0.65$), f_{atm} , f_{soil} , f_{hyd} and f_{veg} are**
 1364 **computed using threshold values of the corresponding metric (Supplementary Methods). The**
 1365 **anomalies are computed by subtracting the climatological mean of 1961-1990 (or a subset of years**
 1366 **during this period depending on the temporal coverage of the input data). The horizontal dashed**
 1367 **lines are zero lines. The shaded areas represent the 95% confidence intervals of multiple data**
 1368 **sources (for VPD and AI) or model results (for DGVMs or ESMs). The ESM results are derived**
 1369 **from CMIP5 under the “historical” (1948-2005) and “RCP4.5” (2006-2100) scenarios. Trends of**
 1370 **each metric and dataset are summarised in Table S5.**
 1371

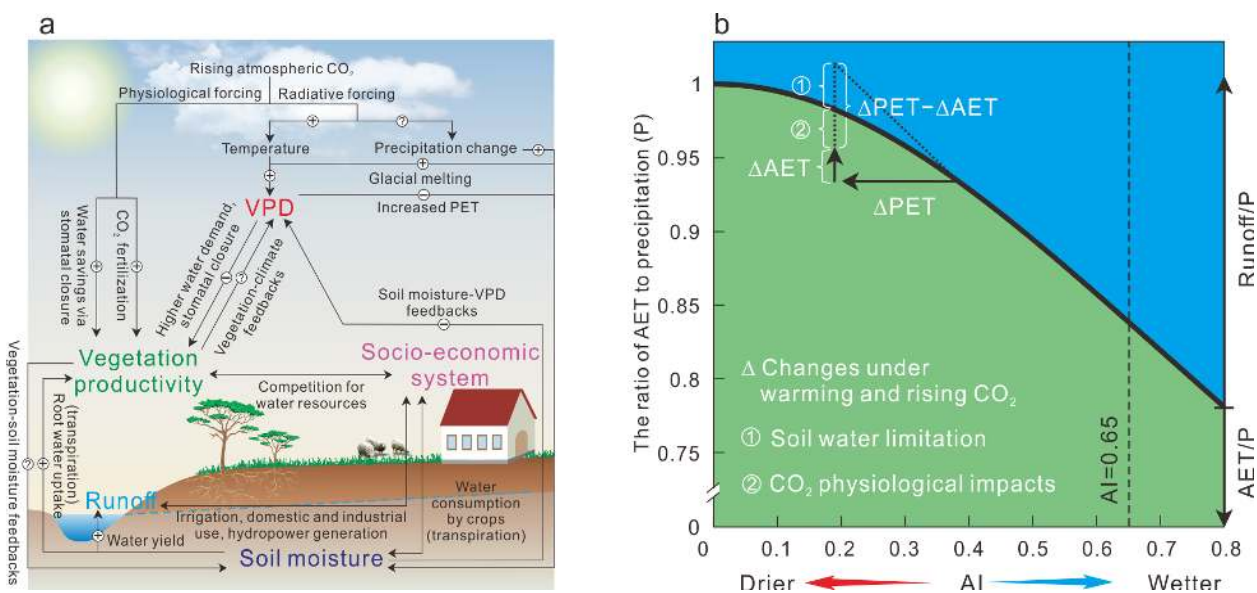


1372

1373 **Figure 3 | Continental assessment of future dryland changes.** Projected future changes in the
1374 fraction of drylands and the four dryland subcategories (dry sub-humid, semi-arid, arid and hyper-
1375 arid; columns) as presented by f_{atm} (**a-e**), f_{AI} (left half of symbols) or $f_{\text{AI_CO}_2}$ (right half of symbols)
1376 (**f-j**), f_{soil} (**k-o**), f_{hyd} (**p-t**) and f_{veg} (**u-y**). For each panel, shown is the difference between dryland
1377 area (as a percentage of the sub-continent area) of a future period (1.5 °C or 2 °C warmer than the
1378 pre-industrial level, or the 2090s; all under the CMIP5 RCP4.5 scenario) and that of the 1961-1990
1379 baseline (under the CMIP5 historical scenario). Continental drylands labelled “I-VI” are marked
1380 with red boxes in the map, panel **z**. For each continent, changes in f_{atm} , f_{soil} , f_{hyd} and f_{veg} are computed
1381 using threshold values of the corresponding metric (Supplementary Methods). **z** | Spatial
1382 distribution of regions where vegetation growth indicates a conversion from drylands to non-
1383 drylands in the near future (for 1.5 °C warmer, 2 °C warmer or the 2090s, relative to 1961-1990),
1384 corresponding to panels **u-y**.

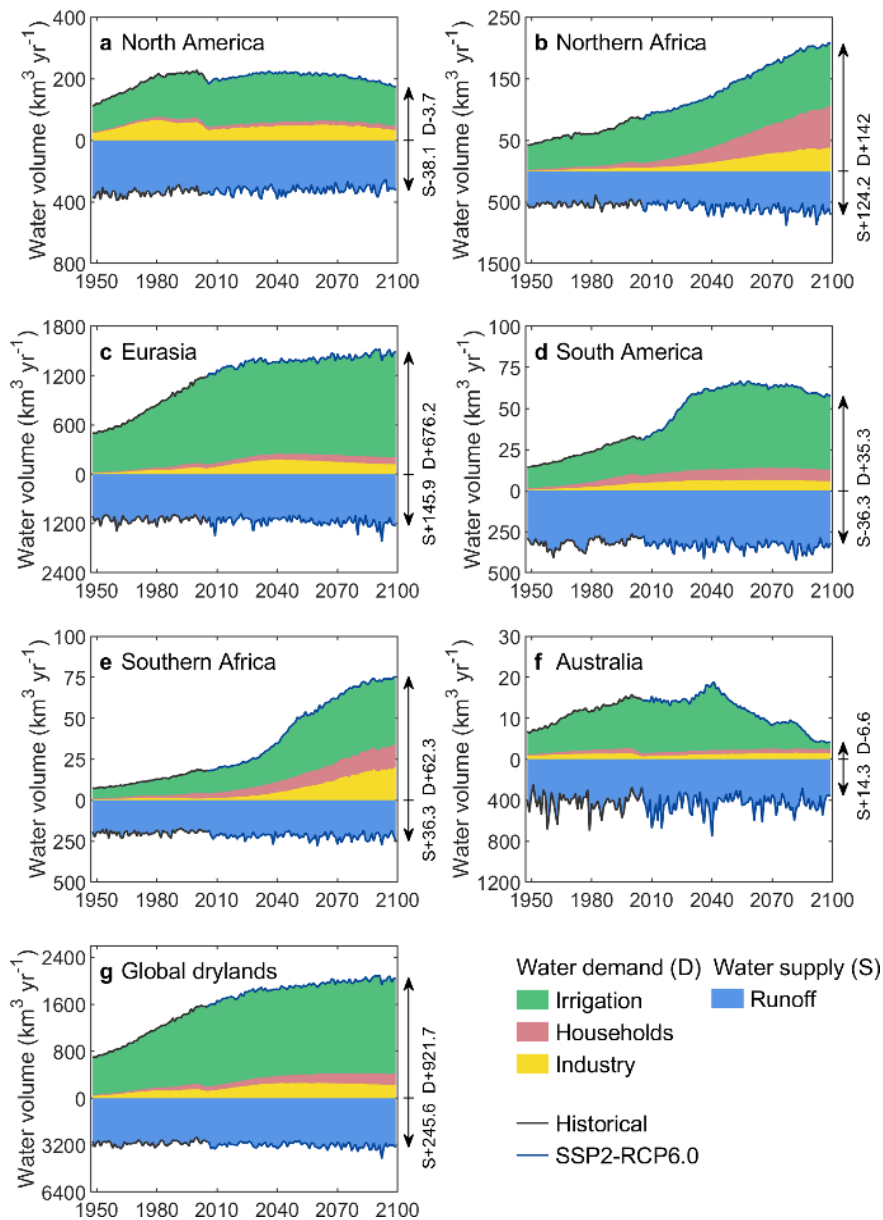


1386 **Figure 4 | Physical and physiological mechanisms for dryland aridity changes.** **a** | Schematic
 1387 representation of processes underlying aridity changes of the atmospheric, hydrological, ecological
 1388 and socio-economic systems, under warming and rising atmospheric CO₂. Circled symbols of ‘-’,
 1389 ‘+’ and ‘?’ represent a negative, positive or potentially unknown sign, respectively, on the quantity
 1390 the corresponding arrow points to. **b** | Mechanisms for the shifting partitioning of precipitation
 1391 between AET and runoff under warming and elevated CO₂. The curve shows the Budyko
 1392 framework^{170,171} that links the partitioning of precipitation (P) into AET (green shaded area) and
 1393 runoff (blue shaded area) to surface aridity level (defined by AI). The symbol ‘Δ’ denotes change
 1394 of the corresponding quantity under warming and elevated CO₂. Under conditions of warming and
 1395 decreasing AI values, the AET increase (vertical black arrow) cannot keep up with the PET increase
 1396 (horizontal black arrow), due to the water limitations and the physiological regulations of plant
 1397 water loss under elevated CO₂.



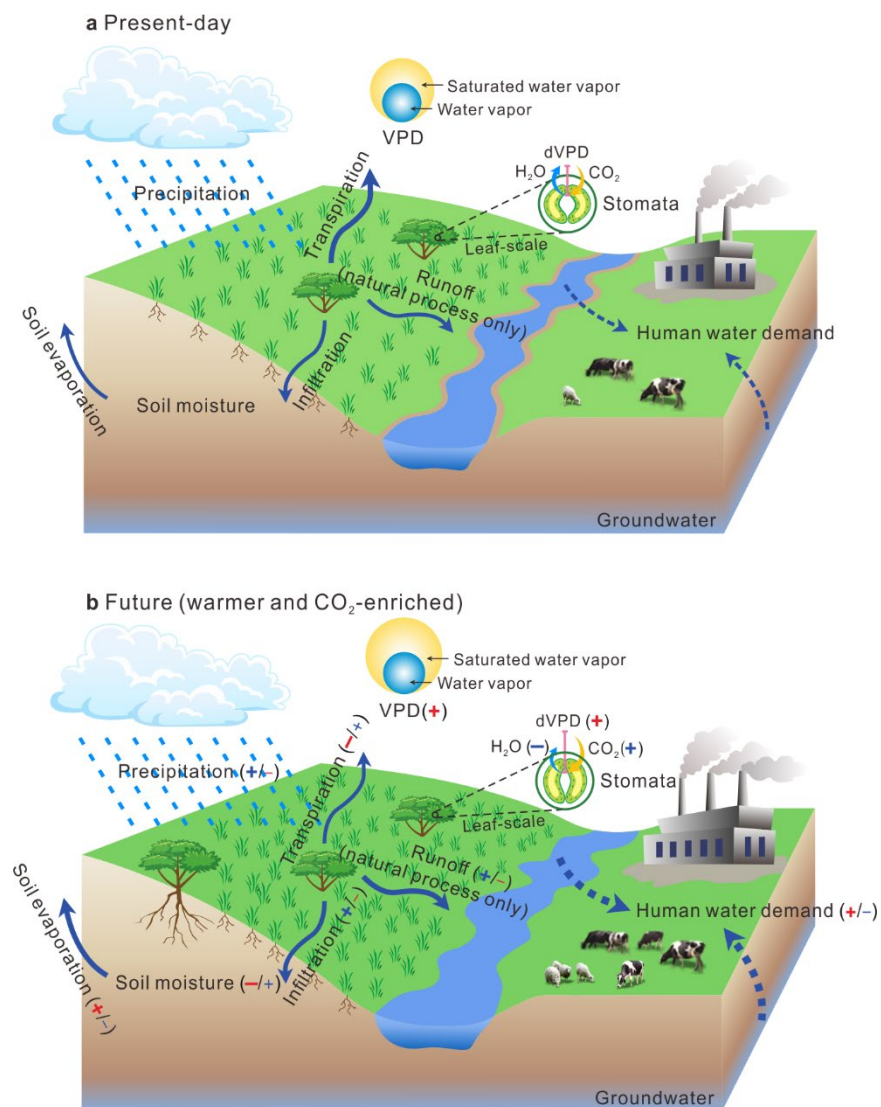
1398
 1399

1400 **Figure 5 | Dryland anthropogenic water stress under climatic and socio-economic changes. a-**
 1401 **f |** Historical and future changes of total anthropogenic water, for the six dryland sub-continent
 1402 displayed in Fig. 3z, respectively. **g** shows the sum of the six dryland sub-continent. The water
 1403 demand (D) is presented as a sum of agricultural, domestic and industrial water withdrawal, and
 1404 the water supply (S) is mainly surface runoff. The y-axis scale is different for D and S. The time
 1405 series are derived from the ensemble mean of three global hydrological models (GHMs, including
 1406 H08, MATSIRO and LPJml) under the SSP2-RCP6.0 scenario. Arrows show the amount of D and
 1407 S during 2090s, with numbers on the right showing the relative changes to the 1961-1990 baseline.



1408

1409 **Figure 6 | Conceptual diagram of future dryland aridity changes. a** Present-day versus **b** future
 1410 aridity conditions of the atmospheric, hydrological, ecological and socio-economic systems over
 1411 drylands. Future changes of dryland ecohydrological variables are based on CMIP5 ESM
 1412 simulations, without accounting for direct human interference. In panel **b**, red symbols of ‘+’ and
 1413 ‘-’ in brackets represent an overall increase and decrease in the corresponding quantity respectively,
 1414 relative to its present-day level. Note that the potential spatial heterogeneity of ecohydrological
 1415 changes is not illustrated in this diagram. The anticipated water demand changes (in dashed arrow)
 1416 of the human society are based on global hydrological model (GHM) simulations.



1417
 1418